

1 **Title**

2 Control of AMPA receptor activity by the extracellular loops of auxiliary proteins

3

4 **Author names and affiliations**

5 Irene Riva*†, Clarissa Eibl*†, Rudolf Volkmer[§], Anna L. Carbone†# and Andrew J. R. Plested†#

6 †Leibniz-Forschungsinstitut für Molekulare Pharmakologie, 13125 Berlin and Cluster of Excellence,

7 NeuroCure, Charité - Universitätsmedizin, 10117 Berlin, Germany

8 [§] Leibniz-Forschungsinstitut für Molekulare Pharmakologie, 13125 Berlin and Charité -

9 Universitätsmedizin Berlin, Campus Berlin Buch, 13125 Berlin

10 *These authors contributed equally to this work

11 #To whom correspondence should be addressed: carbone@fmp-berlin.de (A.L.C.) or

12 plested@fmp-berlin.de (A.J.R.P.)

13

14 **Abstract**

15 At synapses throughout the mammalian brain, AMPA receptors form complexes with auxiliary
16 proteins, including TARPs. However, how TARPs modulate AMPA receptor gating remains poorly
17 understood. We built structural models of TARP-AMPA receptor complexes for TARPs $\gamma 2$ and $\gamma 8$,
18 combining recent structural studies and de novo structure predictions. These models, combined
19 with peptide binding assays, provide evidence for multiple interactions between GluA2 and variable
20 extracellular loops of TARPs. Substitutions and deletions of these loops had surprisingly rich
21 effects on the kinetics of glutamate-activated currents, without any effect on assembly. Critically, by
22 altering the two interacting loops of $\gamma 2$ and $\gamma 8$, we could entirely remove all allosteric modulation of
23 GluA2, without affecting formation of AMPA receptor-TARP complexes. Likewise, substitutions in
24 the linker domains of GluA2 completely removed any effect of $\gamma 2$ on receptor kinetics, indicating a
25 dominant role for this previously overlooked site proximal to the AMPA receptor channel gate.

26 **Introduction**

27 Since the identification of the protein Stargazin, also known as $\gamma 2$, as the prototype
28 transmembrane AMPA receptor regulatory protein (TARP)(1), a broad family of auxiliary proteins
29 for the AMPA receptor have been described (2, 3). These proteins play an essential role in
30 tethering AMPA-type glutamate receptors at the synapse, and also exert complex control over
31 surface expression of functional receptors (4, 5). Auxiliary proteins regulate the function of AMPA
32 receptors, with both positive and negative modulation of gating (6–9), as well as control over
33 permeation and block (10). The range of auxiliary subunit influence over synaptic transmission is
34 compounded by striking regional and cell-type specific expression (11, 12), and a patchwork of
35 interaction patterns (13).

36
37 TARPs and other auxiliary proteins modify the gating and pharmacology of synaptic AMPA
38 receptors (14, 15). The physiological importance of modulation is likely to be the specialization of
39 particular codes of short-term plasticity, in the hippocampus and cerebellum at least (7, 16–18).
40 Recently, antagonists of AMPA receptors that target GluA2– $\gamma 8$ complexes were described (19, 20),
41 further enhancing interest in the molecular basis of complexes of GluA subunits and their auxiliary
42 proteins as potential drug targets.

43
44 Previous studies showed that some of the effects of auxiliary proteins on receptor gating were due
45 to the extracellular domains (21–23). However, several of these studies made use of chimeras with
46 $\gamma 5$, which was presumed to be a null subunit, but which was subsequently shown to modulate
47 gating and conductance of GluA receptors (24). Although some mutations in extracellular portions
48 of TARPs were reported that affect TARP activity, there is no clear indication that these TARPs
49 formed complexes with GluA subunits as well (25). On the other hand, some studies of assembly
50 made use of functional tests to assess the strength of interaction (26). Given the variable
51 stoichiometry of assembly between different TARP isoforms (27, 28), interpreting these data, which
52 combine the strength of association, expression and modulation into a single metric, is difficult.
53 Very recently, a chimeric approach confirmed impressions from structural studies that

54 transmembrane interactions are important for proper assembly, with the TM3 and TM4 segments
55 of $\gamma 2$ and the M1-M3 helices of the AMPA receptor determining complex assembly. However, the
56 C-termini of both the AMPA receptor and TARPs also appear to be involved (29). Despite these
57 insights, there is very little information about the extent to which different domains contribute to
58 gating of complexes (30), and no information about the structural basis of slow modulation,
59 superactivation (37).

60

61 Two of the predominant TARPs in the brain are the auxiliary proteins $\gamma 2$ and $\gamma 8$. In this work, we
62 isolate the extracellular segments of $\gamma 2$ and $\gamma 8$ that are responsible for modulation of gating, and
63 show that these segments act on the receptor via the linkers connecting the ligand binding domain
64 (LBD) and the transmembrane domain (TMD). In so doing, we were able to produce “null” TARPs,
65 which assemble normally but show no modulation of gating. Hereby, we establish mechanisms for
66 the subunit specific modulation of AMPA receptors by auxiliary proteins.

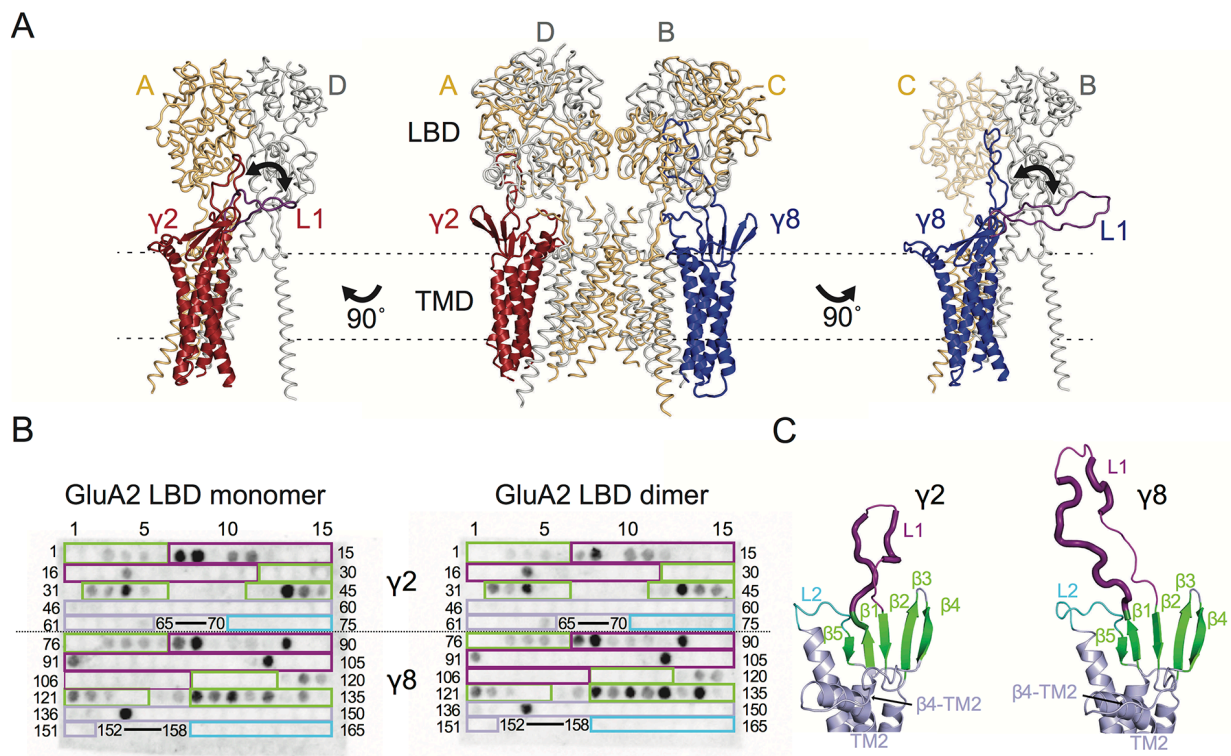
67

68

69 **Results**

70 **A model of auxiliary protein interactions**

71 Previous studies of TARP modulation of AMPA receptors have identified extracellular regions as
72 potential interaction motifs. Crystal structures of Claudins, proteins with close homology to TARPs,
73 enabled a more refined view, defining a folded extracellular “cap” (31–33) that substantially limits
74 the sections of the extracellular portion of TARPs that are able to interact with the AMPA receptor,
75 and therefore the likely range of these interactions. More recently, CryoEM micrographs of GluA2-
76 TARP complexes allowed unambiguous positioning of TARPs at the periphery of the GluA2 pore,
77 and partially resolved the extracellular domains of TARPs (34, 35). The major sequence and
78 structural differences between Claudin and TARP proteins, and between TARPs with different
79 modulatory effects, are found in the variable extracellular loops between $\beta 1$ and $\beta 2$ (Loop 1), and
80 between TM3 and $\beta 5$ (Loop 2). We sought to identify interactions between TARPs and the
81 extracellular regions of the GluA2 receptor on this basis.



82

Figure 1. Modeling and biochemical analysis of AMPA-TARP complexes. A) The middle panel shows TARPs $\gamma 2$ (red) and $\gamma 8$ (blue) positioned between equivalent receptor subunits (A&D and B&C) based on the cryo-EM complex structure (5kk2). The predicted flexible extracellular L1 of $\gamma 8$ is longer than in $\gamma 2$ enabling it to reach more extensive regions of the receptor. To account for its flexibility we modeled L1 either between the LBD dimer (colored like the respective TARP) or underneath the lower lobe of the LBD (purple; left panel for $\gamma 2$, right panel for $\gamma 8$). L1 might engage in different interactions with the LBD depending if located next to the inter-dimeric LBD interface (between subunits A & B or A & D; see Figure 1 – Figure supplement 1A). **B)** TARP peptide spotted membranes incubated with either monomeric (left panel) or dimeric GluA2 LBD (right panel). Interacting peptides give a dark spot on the membrane when developed. The colored boxes indicate where the peptides are located in the TARPs (from $\beta 1$ to L2) which is further illustrated in the structural models of $\gamma 2$ and $\gamma 8$ in panel C and Figure 1 – Figure supplement 1C. Quantitation of the spot arrays is found in Figure 1 – Source Data 1. **C)** Close up view on the modeled extracellular region of $\gamma 2$ (left) and $\gamma 8$ (right). Secondary structure elements are shown in cartoon representation with β -sheets colored green, extracellular loop 1 in purple and loop 2 in cyan. Positive peptide hits in L1 are indicated by thicker loop-representation.

83 To understand the scope of TARP interactions with the AMPA receptor, we began by modeling the
84 loops of $\gamma 2$ and $\gamma 8$ into a hybrid structure composed of Claudins and GluA2. Comparing these
85 hybrid complexes to CryoEM electron density maps suggested that a range of interaction sites with
86 the LBD-TMD linkers and D2 domains of the LBD are possible (Figures 1A and Figure 1 – Figure
87 supplement 1A). Whereas TARP loop 2 (L2) engages in the receptors pore four-fold symmetry,
88 loop 1 (L1) reaches up to the two-fold symmetry of the LBD layer. In other words, while L2 can
89 interact four times in the same way with the receptor (Figure 1 – Figure supplement 1B), L1 has at
90 least two distinct modes of interaction depending on to which receptor subunits the TARP is
91 adjacent (subunit A-D and B-C, Figure 1A, or A-B and C-D, Figure 1 – Figure supplement 1A). The
92 variable loop 1 is not resolved in structures to date, consistent with it being a flexible modulatory
93 element. Superactivation of GluA2 receptors resembles strongly the slow modulation of AMPA
94 receptors by particular allosteric modulators that bind at the dimer interface (36, 37). We reasoned
95 that extracellular loop interactions that stabilized the superactive state could preferentially target
96 the GluA2 LBD dimer. To test this hypothesis, we composed an overlapping library of hexameric
97 peptides based on extracellular sections of TARPs, targeting the long loop 1 of $\gamma 2$ and $\gamma 8$, and
98 other potential interacting sites (Figure 1 – Figure supplement 1C). Because the active dimer of
99 LBDs ought to be intact for superactivation, we compared the interactions of our peptide library
100 between the GluA2 LBD (flip form) and LBDs harboring the L483Y substitution, which greatly
101 increases dimer formation in solution.

102

103 Repeated peptide mapping array assays indicated no clear preference for either monomeric or
104 dimeric GluA2 LBD. However, in accordance with our hypothesis the majority of the L1 of both $\gamma 2$
105 and $\gamma 8$ contain hits in the peptide mapping array, indicating direct interaction with the receptor LBD
106 (Figures 1B and C Figure 1 – Figure supplement 1C), albeit in conditions lacking the usual steric
107 constraints of the complex. In the recent cryo-EM structures of the GluA2-TARP complex a
108 possible interaction between a conserved negatively charged region located on the TARP $\beta 4$ -TM2
109 loop and the KGK motif in the lower lobe of the GluA2 LBD was predicted (34, 35). Thus we also
110 tested for this potential interaction in the peptide mapping array but found no hits. A functional test

111 of removing the acidic residues in this patch made $\gamma 2$ into a much stronger modulator of AMPAR
112 gating, with the steady-state current and superactivation both doubled (Figure 1 – Figure
113 supplement 2). This result suggested that if interactions of the acidic patch with the receptor alter
114 function, they actually inhibit the action of $\gamma 2$. However, other sites have a dominant effect in the
115 positive modulation of gating.

116

117 We also tested L2 of $\gamma 2$ and $\gamma 8$ for possible interactions with the LBDs because of its conserved
118 charged features (4 and 7 charges), which are less prominent in $\gamma 5$ and $\gamma 7$ (3 and 1 charges
119 respectively). Considering L2 being positioned distant underneath the LBD (around 15Å, measured
120 between Ca of GluA2 P717 and $\gamma 2$ K170 in the complex from PDB code: 5kbu (34) in the cryo-EM
121 structures, it was not surprising that we found no interaction between L2 peptides and the GluA2
122 LBD. According to our GluA2-TARP models, in both $\gamma 2$ and $\gamma 8$ L2 is positioned between the S1-M1
123 and S2-M4 linkers (Figure 1 – Figure supplement 1A and B), which are outside the realms of our
124 GluA2 LBD construct.

125

126 **Modulation of fast AMPA receptor gating by TARP L1 and L2 segments**

127 To investigate the role of the extracellular domain of TARPs in controlling AMPA receptor
128 activation, we made a series of chimeras and deletion mutants between $\gamma 2$ and $\gamma 8$. We first
129 targeted the long loop in the first extracellular segment L1 (Figure 1) that has markedly different
130 lengths and sequence content across the TARP family and its homologs. We also investigated the
131 role of the shorter unstructured region in the second extracellular segment L2 (Figure 1), which is
132 poised to interact with the LBD-TMD linkers of the AMPA receptor.

133

134 We first swapped L1 between $\gamma 2$ and $\gamma 8$ (Figures 2A and Figure 1 – Figure supplement 3), and
135 assessed effects on desensitization. Although $\gamma 2$ and $\gamma 8$ apparently affect AMPA receptor
136 desensitization similarly, $\gamma 8$ slows down entry to desensitization more than $\gamma 2$ ($60 \pm 5 \text{ s}^{-1}$ and $40 \pm$
137 5 s^{-1} , $n = 24$ and 9 , for $\gamma 2$ and $\gamma 8$, respectively; Table 1). These chimeras exhibited asymmetric
138 effects on desensitization. When activated by 10 mM glutamate, the chimera of $\gamma 2$ with L1 from $\gamma 8$

139 had steady-state current of $50 \pm 5 \%$ ($n = 30$; Figures 2A and D and Table 1), twice as large as $\gamma 2$
 140 alone ($25 \pm 2 \%$, $n = 24$ patches), and the rate of entry to desensitization was approximately halved
 141 ($35 \pm 5 \text{ s}^{-1}$, $n = 30$; Figure 2C and Table 1). In contrast, the $\gamma 8$ chimera with L1 from $\gamma 2$ maintained
 142

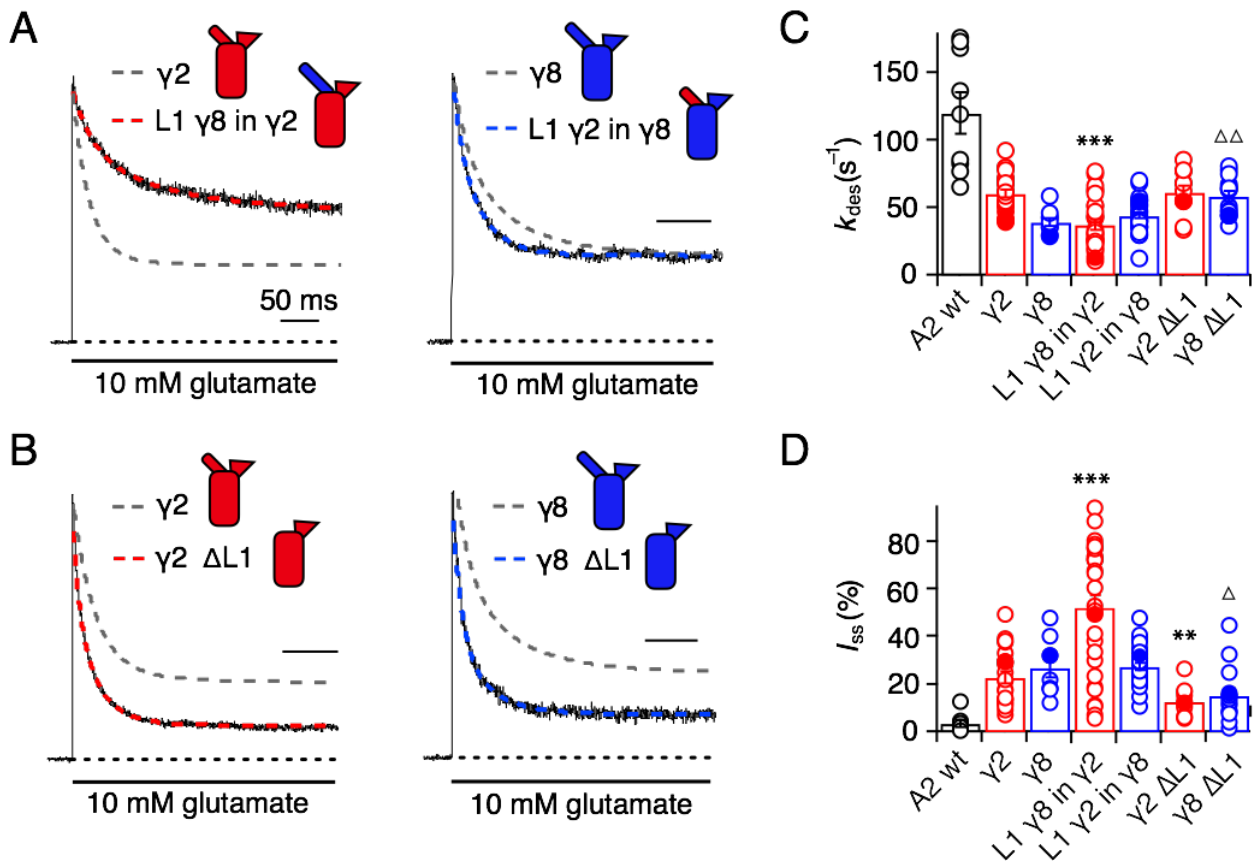


Figure 2. Desensitization properties of $\gamma 2$ and $\gamma 8$ L1 mutants. **A)** Representative traces from L1 $\gamma 8$ in $\gamma 2$ (red) and L1 $\gamma 2$ in $\gamma 8$ (blue) coexpressed with GluA2 in response to a 500 ms pulse of 10 mM Glutamate ($k_{des} = 13$ and 55 s^{-1} ; $I_{ss} = 50$ and 30% , respectively). Example traces recorded from the parent TARPs coexpressed with GluA2 are shown in grey for comparison ($k_{des} = 41$ and 30 s^{-1} ; $I_{ss} = 30$ and 30% , for $\gamma 2$ and $\gamma 8$, respectively). **B)** Representative traces from $\gamma 2 \Delta L1$ (red) and $\gamma 8 \Delta L1$ (blue) coexpressed with GluA2 in response to a 500 ms pulse of 10 mM Glutamate ($k_{des} = 55$ and 45 s^{-1} ; $I_{ss} = 10$ and 15% , respectively). The wild type constructs coexpressed with GluA2 are shown as dashed lines for comparison. **C)** Bar graph summarizing the effects of the L1 mutation on the desensitization kinetics. **D)** Bar graph summarizing the effects of the loop1 mutations on the steady state current of the complexes. Currents were recorded at +50 mV in the presence of $50 \mu\text{M}$ spermine in the pipette solution. For panels C and D, Filled symbols correspond to the traces shown in A) and B). *** $p < 0.001$, ** $p < 0.01$, against $\gamma 2$; $\Delta p < 0.05$, $\Delta\Delta p < 0.01$, against $\gamma 8$. Source data for panels C & D is found in Table 1 – Source Data 1. Error bars represent s.e.m.

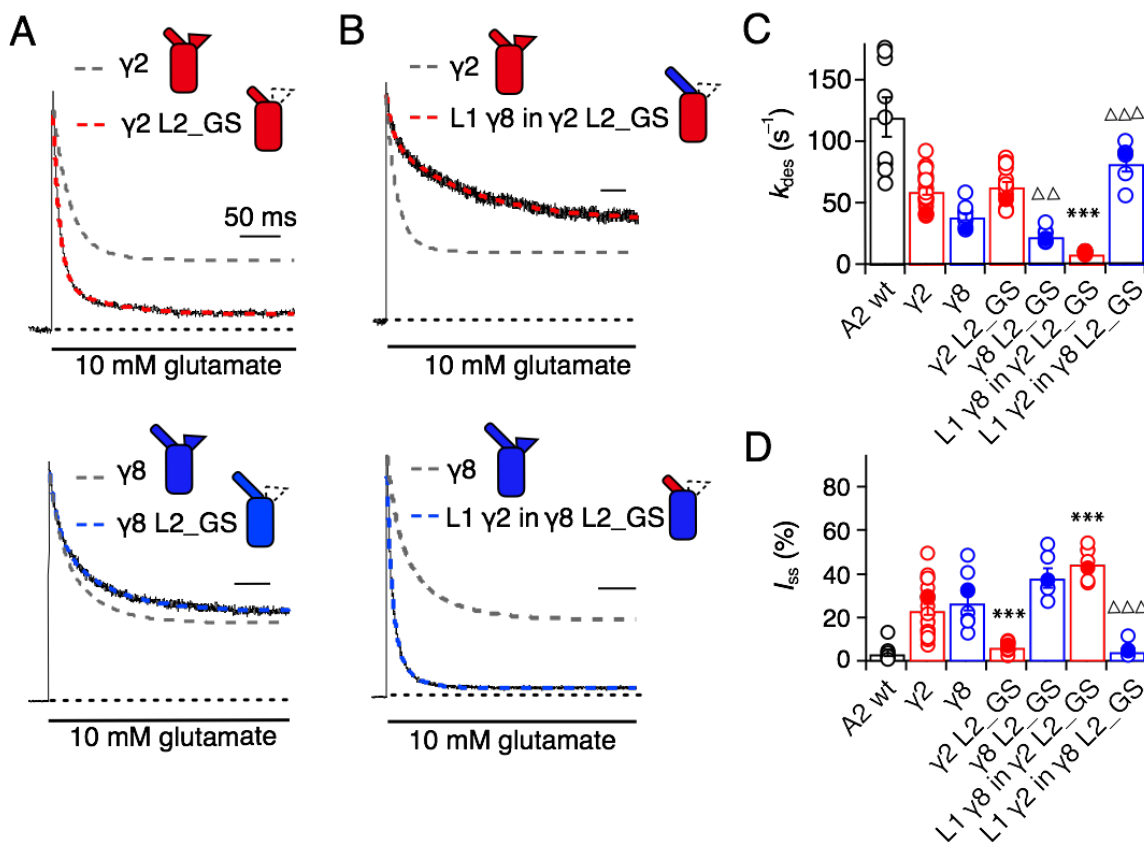
143 the original desensitization behavior of the parent TARP ($45 \pm 1 \text{ s}^{-1}$, $n = 28$; Figures 2A and C and
144 Table 1). Deletion of L1 from $\gamma 2$ and $\gamma 8$ approximately halved the steady state current (15 ± 2 and
145 $15 \pm 3 \%$, $n = 11$ and 15 , for $\gamma 2 \Delta L1$ and $\gamma 8 \Delta L1$, respectively; Figures 2B and D and Table 1), with
146 a barely detectable speeding up of entry to desensitization ($60 \pm 5 \text{ s}^{-1}$, $n = 11$ and 15 , for $\gamma 2 \Delta L1$
147 and $\gamma 8 \Delta L1$, respectively; Figures 2B and C and Table 1). These results suggested that L1 can
148 influence desensitization of complexes, as shown recently for GSG1L (30) but the absence of a
149 simple exchange in desensitization behavior suggested that this loop functions in concert with
150 other modulatory elements.

151

152 Seeking a further explanation for the modulation of desensitization by TARPs, we investigated the
153 effects of altering the 8-residue stretch in the second extracellular segment of TARPs (L2), which
154 connects TM3 to $\beta 5$ in the extracellular domain. Replacement of the L2 segment with a flexible
155 Gly-Ser linker, predicted to be of sufficient length not to disrupt the overall structure of the
156 extracellular domain, had a striking effect on $\gamma 2$. The rate of entry to desensitization was still slower
157 than in receptors formed of GluA2 wild type (WT) alone ($65 \pm 5 \text{ s}^{-1}$ and $120 \pm 15 \text{ s}^{-1}$, $n = 15$ and 9
158 patches for A2 + $\gamma 2$ L2_GS and A2 WT, respectively; Figures 3A and C and Table 1), but the
159 steady state current was reduced to the level of receptors without any TARP present ($5 \pm 1 \%$ and
160 $5 \pm 1 \%$, $n = 15$ and 9 for A2 + $\gamma 2$ L2_GS and A2 WT, respectively; Figures 3A and D and Table 1).
161 In contrast, there was no detectable effect on $\gamma 8$ of mutating this loop, except for a further slowing
162 down of the desensitization rate ($k_{\text{des}} = 25 \pm 5 \text{ s}^{-1}$, $I_{\text{ss}} = 40 \pm 4\%$, $n = 6$, for $\gamma 8$ L2_GS; Figures 3A,
163 C and D and Table 1).

164

165 Even more striking were results of coexpression of a chimera of $\gamma 2$ with the GS-linker replacing L2,
166 but harboring the long L1 loop of $\gamma 8$. This chimera massively slowed entry to desensitization,
167 producing complexes about 10-fold slower than receptors without any TARP ($k_{\text{des}} = 10 \pm 0.5 \text{ s}^{-1}$, n
168 $= 7$; Figures 3B and C and Table 1), and increased the steady state current during a 500 ms pulse
169 of glutamate ($45 \pm 3\%$, $n = 7$; Figures 3B and D and Table 1). Making the inverse chimera (L1 from
170 $\gamma 2$ in $\gamma 8$, with the GS-linker replacing L2) effectively nullified the modulatory activity of $\gamma 8$.



171

172 The steady-state current was the same magnitude as for receptors that did not have $\gamma 8$ ($5 \pm 1\%$, n

173 = 6; Figures 3B and D and Table 1), and the rate of entry to desensitization (85 ± 20 s $^{-1}$, $n = 6$;

174 Figures 3B and C and Table 1) was closer to that of wild-type GluA2 than for the $\gamma 2$ L2_GS

175 chimera (see Table 1).

176 Although we performed all measurements at +50 mV, isolating heavily TARPed receptors by
177 selecting for complexes with strong relief of polyamine block, we were concerned that some of the
178 effects that we saw (particularly reduced or absent modulation) could be due to an altered
179 stoichiometry of complexes, perhaps due to poor chimera expression. To assess this possibility,
180 we measured the G-V relations for all the chimeras and deletion mutants (Figure 2 – Figure
181 supplement 1). Importantly, all mutants gave responses that were strongly reduced in rectification,
182 indicating that complex formation was normal. Broadly, each chimera closely followed the
183 polyamine relief induced by the parent TARP, with $\gamma 2$ chimeras producing populations of receptors
184 that exhibited a greater rectification index than those based on $\gamma 8$ (Figure 2 – Figure supplement
185 1).

186

187 **Superactivation of AMPA-TARP complexes**

188 TARPs induce a subtype-specific superactivation of the GluA2 homomeric receptor. $\gamma 8$ is a much
189 stronger modifier of this slow gating mode than $\gamma 2$ (36, 37). We investigated the role of the
190 extracellular domain in superactivation using the same set of TARP mutants, but using 7-second
191 applications of glutamate to measure the equilibrium level reached following superactivation. Our
192 hypothesis was that the difference in superactivation between $\gamma 2$ and $\gamma 8$ would be specified by the
193 sequence element most divergent between these two TARPs, L1.

194

195 In the chimeras swapping loop 1 between $\gamma 8$ and $\gamma 2$, the results were asymmetric (Figure 4). That
196 is, loop 1 from $\gamma 8$ could transfer the same degree of superactivation to $\gamma 2$ (L1 $\gamma 8$ in $\gamma 2$, $27 \pm 6\%$, n
197 = 10 ; Figures 4A and C and Table 1) but the reverse swap could not reduce superactivation to the
198 level of $\gamma 2$ (L1 $\gamma 2$ in $\gamma 8$, $16 \pm 1\%$, $n = 16$; Figures 4B and C and Table 1). The reason for this
199 asymmetry became clear when we recorded complexes from which we removed L1 altogether
200 from each TARP residual superactivation of 6 ± 2 and $16 \pm 3\%$ (for $\gamma 2$ and $\gamma 8$, respectively, $n = 6$;
201 Table 1) were still present in the absence of L1. Therefore, although loop 1 can contribute to

202 superactivation, and increase it over baseline levels, it is not the only element of TARPs driving this
 203 effect.
 204

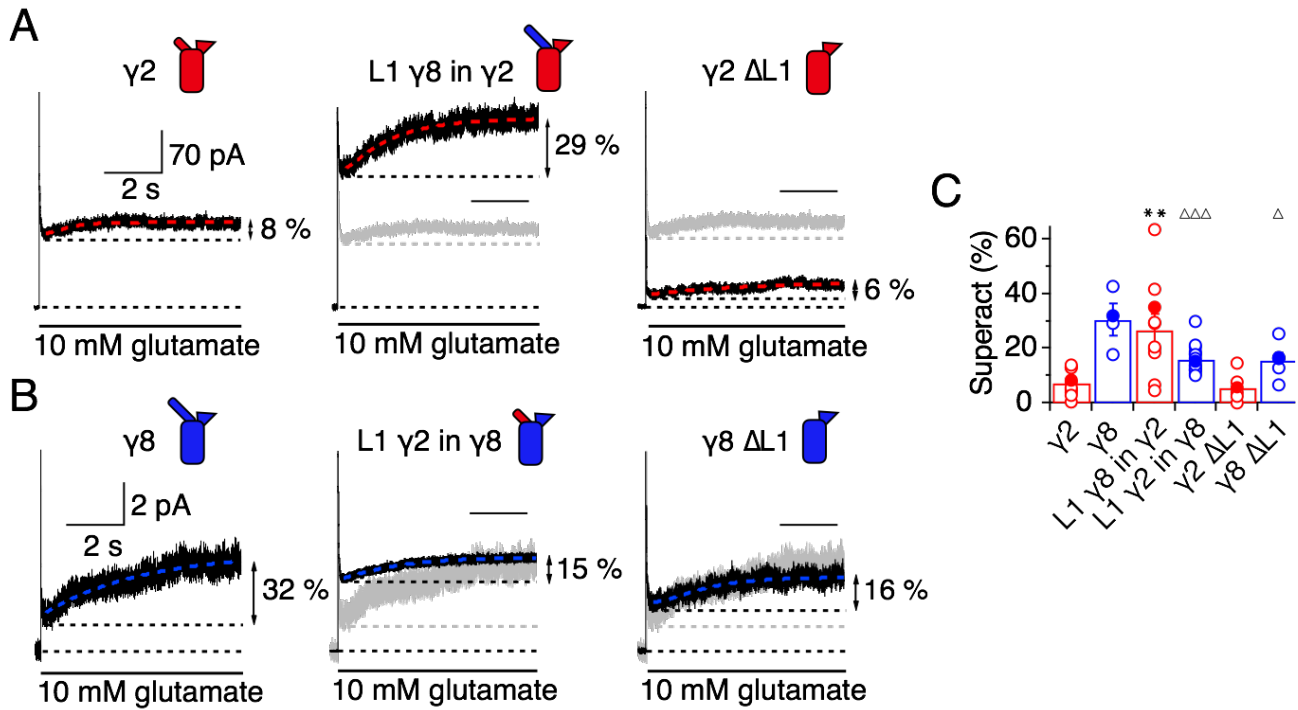


Figure 4. L1 modulates the extent of TARP-mediated superactivation. A) Example traces of $\gamma 2$ wild-type and L1 mutants in response to 7 sec application of 10 mM glutamate. During prolonged application of 10 mM Glutamate $\gamma 2$ induced superactivation of GluA2 receptors, shown as an increase in the steady state current (8% in the example shown, *left panel*). The extent of superactivation was increased by 3-fold when L1 was replaced with that of $\gamma 8$ (*central panel*). Removing loop1 in $\gamma 2$ did not affect superactivation much (*right panel*). **B)** $\gamma 8$ showed much bigger superactivation than $\gamma 2$ during long glutamate exposure (*left panel*). Shortening loop 1 by replacing it with that of $\gamma 2$ or removing it decreased superactivation by 2-fold (*central and right panel*). **C)** Bar graph summarizing the effects of the loop1 mutations on receptor superactivation. Currents were recorded at +50 mV in the presence of 50 μ M spermine in the pipette solution. Filled symbols correspond to the traces shown in A) and B) ** $p < 0.01$, against $\gamma 2$; $\Delta\Delta\Delta p < 0.001$, $\Delta p < 0.05$, against $\gamma 8$. Source data for panel C is found in Table 1 – Source Data 1. Error bars represent s.e.m.

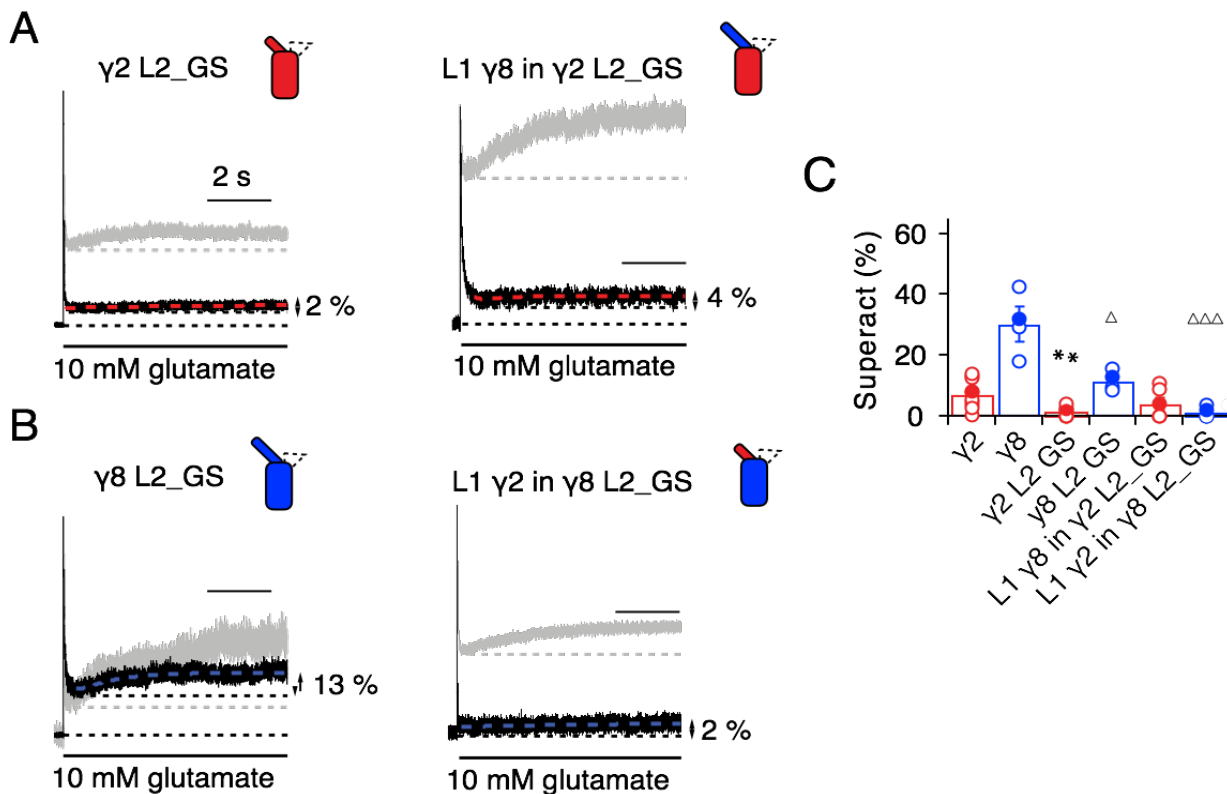


Figure 5. Superactivation of $\gamma 2$ and $\gamma 8$ L2 mutants. **A)** Neutralizing L2 from $\gamma 2$ strongly reduced $\gamma 2$ -mediated superactivation (*left panel*). On this background, L1 from $\gamma 8$ induced only minimal superactivation (*right panel*). The grey traces represent WT $\gamma 2$ (*left*) and L1 $\gamma 8$ in $\gamma 2$ (*right*). **B)** Removing L2 in $\gamma 8$ decreased superactivation 2.5 fold (*left panel*). Introducing L1 from $\gamma 2$ on this background practically abolished superactivation (*right*). The grey traces represent WT $\gamma 8$ (*left*) and L1 $\gamma 2$ in $\gamma 8$ (*right*). **C)** Bar graph of the effects of the L2 neutralization and L1 chimeras on superactivation. Filled symbols correspond to the traces shown in A) and B). ** $p < 0.01$, against $\gamma 2$; $\Delta\Delta\Delta p < 0.001$, $\Delta p < 0.05$, against $\gamma 8$. Source data for panel C is found in Table 1 – Source Data 1. Error bars represent s.e.m.

205 Given the residual superactivation that we saw in the absence of loop 1, we reasoned that loop 2
 206 could play a role in receptor superactivation (Figure 5). We measured responses to 10 mM
 207 glutamate for the L2_GS mutants of $\gamma 2$ and $\gamma 8$ and found substantially reduced superactivation
 208 (1.3 ± 0.6 and 12 ± 2 %, $n = 8$ and 4 , respectively; Table 1).

209
 210 Even more strikingly, the same TARP mutants with loop 1 swapped had a further reduced effect.
 211 The loop 1 from $\gamma 2$ in the L2_GS mutant of $\gamma 8$ had almost negligible superactivation, reduced by
 212 ~ 15 -fold from wild-type $\gamma 8$, to about 1 ± 0.7 % ($n = 6$; Figures 5B and C and Table 1). Taking into
 213 account the lack of steady-state current, fast desensitization and similar deactivation kinetics to

214 wild-type GluA2 alone that we observed in patches containing complexes of GluA2 with the L1 $\gamma 2$
215 in $\gamma 8$ L2_GS mutant, we classed this chimera as a kinetic null of $\gamma 8$.

216

217 The TARP chimeras that exhibited the least power to slow desensitization kinetics and to stabilize
218 active states were those that replaced charged residues in the L2 segment, and from which we
219 either deleted L1, or included the short loop from $\gamma 2$. These observations guided our construction
220 of a kinetically-null $\gamma 2$. We reasoned that a $\gamma 2$ chimera lacking L1 and with a GS-linker replacing L2
221 should associate normally with GluA2 but might have no kinetic effect at all on the receptor
222 complexes. Indeed, $\gamma 2 \Delta L1$ L2_GS associated normally into the receptor complex (as assessed by
223 relief of polyamine block, Figures 6A and B) but this mutant $\gamma 2$ was highly deficient in modulating
224 gating of GluA2. Superactivation, and the increase in steady state current were absent in these
225 complexes (superactivation = 0 %; $I_{ss} = 2 \pm 1$ %, $n = 4$ and 5, respectively; Figures 6C and D and
226 Table 1). Somewhat surprisingly, the deletion of L1 from $\gamma 8$ on the L2-GS background retained a
227 larger steady state current than the chimera that included the L1 segment of $\gamma 2$ ($I_{ss} = 5 \pm 1$ % and
228 10 ± 5 %, $n = 6$ and 5, for L1 $\gamma 2$ in $\gamma 8$ L2_GS and $\gamma 8 \Delta L1$ L2_GS, respectively; Figures 5B and C,
229 6E and G and Table 1) and a small superactivation (3 ± 1 %, $n = 4$; Figure 6A and Table 1).

230

231 **L2 controls gating through interaction with linkers proximal to the channel gate**

232 From our models, a range of sites on GluA2 could interact with L1, including the KGK motif in the
233 LBD (30, 38). Substitutions at L2 of $\gamma 2$ and $\gamma 8$ had profound effects on gating of TARP complexes
234 and are well placed to interact with gating machinery (Figure 1A and S1B). Particularly, we
235 expected from our structural models and other available structural data (34, 35) that L2 should
236 interact with the S1-M1 linker and the S2-M4 linker in the AMPA receptor. The L2 sequence has an
237 alternating charge motif that is mirrored in two parts of the GluA2 linkers 508-510 and 781-783.
238 These segments are immediately adjacent to the TARP L2 in all four subunits.

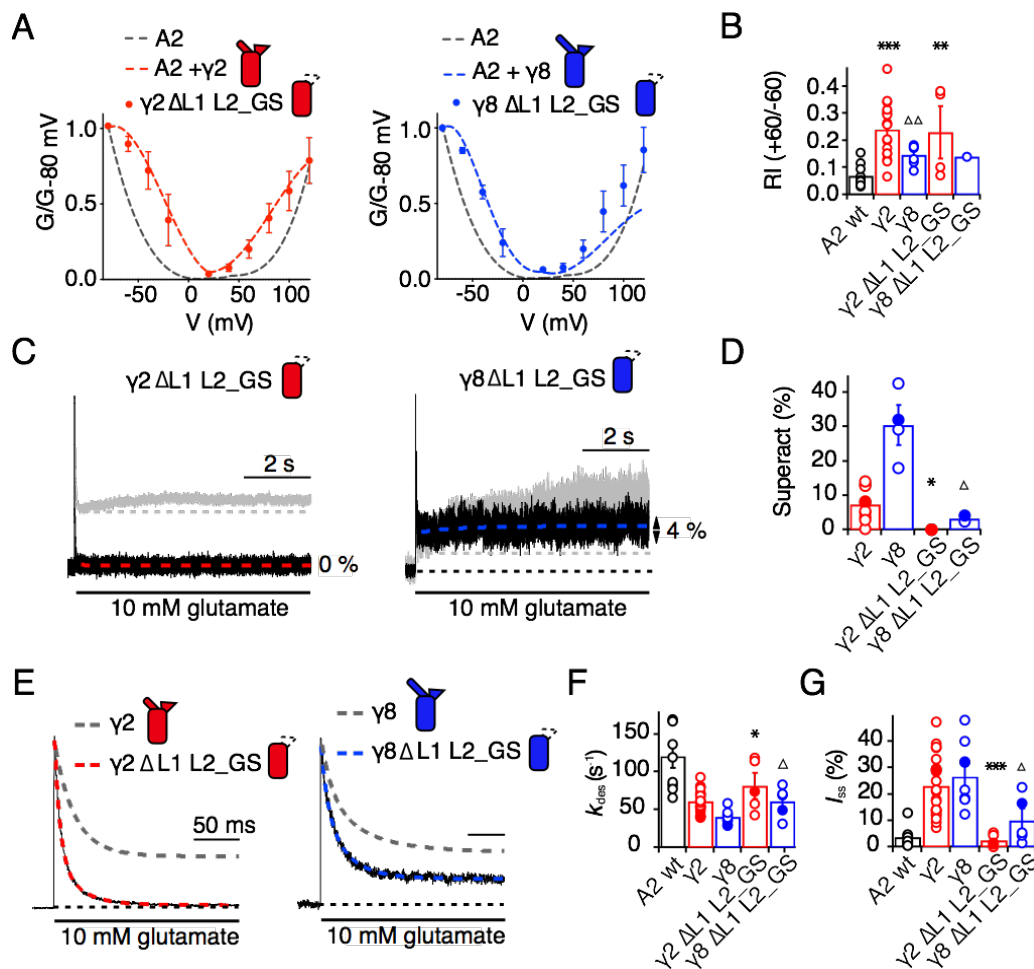


Figure 6. Eliminating L1 and L2 removes modulation by $\gamma 2$. **A)** Mutation of both L1 and L2 in $\gamma 2$ (left panel, red) and $\gamma 8$ (right, blue) did not change association of TARPs with AMPA receptors, as assessed by the G-V curve. GluA2 WT is shown in grey. **B)** Bar graph summarizing the rectification index of the dual loop mutations. **C)** Example traces of $\gamma 2 \Delta L1 L2_GS$ (left) and $\gamma 8 \Delta L1 L2_GS$ (right) in response to 7 sec application of 10 mM glutamate. Corresponding wild-type TARPs are shown as dashed lines. **D)** Bar graphs summarizing the effects of the dual loop mutation in $\gamma 2$ (red) and $\gamma 8$ (blue) on superactivation. **E)** Representative traces from $\gamma 2 \Delta L1 L2_GS$ (left) and $\gamma 8 \Delta L1 L2_GS$ (right) coexpressed with GluA2 in response to a 500 ms pulse of 10 mM Glutamate ($k_{des} = 74$ and 50 s^{-1} $I_{ss} = 1.5$ and 16% , respectively). Currents from the parent TARPs are shown in grey for comparison. **F)** Bar graphs summarizing the effects of the dual loop mutation in $\gamma 2$ (red) and $\gamma 8$ (blue) on desensitization decay. **G)** Bar graph summarizing the effects of the double loop mutation on the steady state current of the complexes. Currents were recorded at +50 mV in the presence of $50 \mu\text{M}$ spermine in the pipette solution. For panels D, F and G, filled symbols correspond to the traces shown in C) and E). *** $p < 0.001$, ** $p < 0.01$, * $p < 0.05$, against $\gamma 2$. Source data for panel B is found in Figure 6 – Source data 1. Source data for panels D, F & G is found in Table 1 – Source Data 1. Error bars represent s.e.m.

240 Replacement of 508QKS510 to GAG in the S1-M1 linker (GluA2 508GAG510, Figure 7A) produced
241 a GluA2 receptor with normal kinetics and that associated normally with $\gamma 2$ and $\gamma 8$ (Figure 7 –
242 Figure supplement 1). Strikingly, in complexes with WT $\gamma 2$, this mutant phenocopied the
243 neutralizing truncation of L2 in TARPs well (see Figure 3), abolishing superactivation and reducing
244 the steady state current (0% and $10 \pm 5\%$, $n = 3$ and 4, for superactivation and I_{ss} , respectively;
245 Figures 7C-E and Table 1). In contrast, a point mutant K509A, also with normal gating (Figure 7 –
246 Figure supplement 1), was more strongly modulated by $\gamma 2$, providing further indication that a
247 second site was potentially involved (Figure 7E and Table 1). Our model suggested that the S2-M4
248 linker of GluA2 was equally well positioned to interact with L2 from $\gamma 2$. To test the importance of
249 the alternating charges in the S2-M4 linker, we made another triple mutation replacing 781KEK783
250 to GSG (GluA2 781GSG783, Figure 7B). This mutant again had normal kinetics in the absence of
251 $\gamma 2$ (Figure 7 – Figure supplement 1), but also exhibited a reduced steady state current and
252 negligible superactivation ($10 \pm 1\%$ and $2 \pm 0.5\%$, $n = 9$ and 8, for I_{ss} and superactivation
253 respectively; Figures 7C-E and Table 1). Importantly, the combination of these two triple mutants,
254 abolished the entire modulatory effect of $\gamma 2$ on the AMPA receptor, reducing superactivation and
255 the instantaneous steady-state current to the same level as GluA2 in the absence of TARP (0 %
256 and $5 \pm 1\%$, $n = 4$ and 8, for superactivation and I_{ss} , respectively; Figures 7C-E and Table 1). This
257 mutant receptor retained ostensibly normal gating and association to TARPs (Figure 7 – Figure
258 supplement 1), despite the absence of gating modulation.

259

260 To discern whether the loss of modulation occurred because the linker sites are the primary
261 interaction site, or whether the linkers both interact with TARPs and transmit upstream modulation
262 from sites in the LBD, we assessed modulation by $\gamma 8$ and related chimeras. The propensity of $\gamma 8$
263 to modulate gating of the double linker mutant (GluA2 GAG/GSG) was reduced, but robust
264 superactivation could still be observed ($25 \pm 5\%$, $n = 5$, Figure 7 and Table 1). Given this result,
265 which suggested that L1 could still modulate gating of complexes, we hypothesized that the $\gamma 2$
266 chimera incorporating the L1 of $\gamma 8$ should also modulate the double linker mutant. This chimera
267 could not produce superactivating complexes ($2 \pm 2\%$, $n = 4$, Figures 7D and E, as for the $\gamma 2$

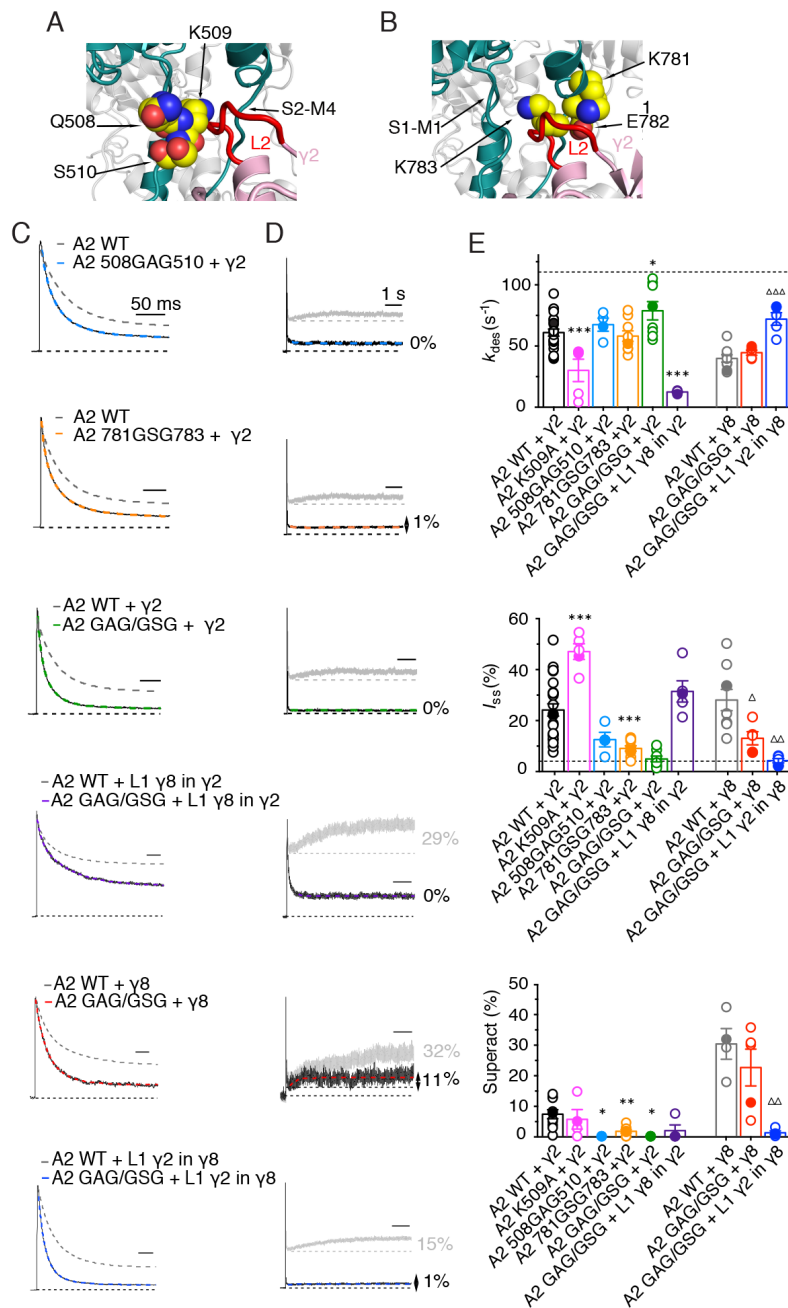


Figure 7. The LBD-TMD linkers are the key sites for modulation of AMPA receptor gating by TARPs. A) Residues in the S1-M1 linker (Gln508, Ser509, and Lys510 represented as yellow atomic spheres) are in close proximity to the L2 of TARPs (L2 of $\gamma 2$ is shown in red). **B)** Residues in the S2-M4 linker (Lys781, Glu782 and Lys783) predicted to interact with L2 are labeled and shown as yellow atomic spheres. **C)** Example responses from linker mutants coexpressed with $\gamma 2$, $\gamma 8$ and loop 1 chimeras to 500 ms 10 mM Glutamate. **D)** Representative responses from linker mutants coexpressed with $\gamma 2$, $\gamma 8$ and loop 1 chimeras to a 7 sec pulse of 10 mM Glutamate. The extent of superactivation is indicated. **E)** Bar graphs summarizing the desensitization properties (*top panel*), steady state current (*central*) and superactivation (*bottom*). Colors are as in panel C. Filled symbols correspond to the traces shown in panels C and D. *** $p < 0.001$, ** $p < 0.01$, * $p < 0.05$, against $\gamma 2$; $\Delta\Delta\Delta p < 0.001$, $\Delta p < 0.05$, against $\gamma 8$. Source data for panel E is found in Table 1 – Source Data 1. Error bars represent s.e.m.

269 chimera lacking L2 interactions, L1 $\gamma 8$ in $\gamma 2$ L2_GS, Figure 5A) but retained the slow desensitizing
270 behavior due to L1 ($k_{des} = 12 \pm 0.5$, $n = 5$, Figure 7E and Table 1).

271

272 In coherence with our previous results, mutation of the GluA2 linkers ablated the effect of the $\gamma 8$
273 chimera with L1 from $\gamma 2$ to modulate the kinetics of complexes, reducing the steady state current
274 and superactivation to the same levels as GluA2 wild-type in the absence of TARP ($I_{ss} = 4 \pm 1$ %,
275 superactivation = 1 ± 1 %, $n = 5$ and 4, Figure 7E and Table 1). Therefore, in the absence of the
276 long L1, $\gamma 8$ fails to modulate GluA2 when the S1-M1 and S2-M4 linker interaction sites are
277 removed (again consistent with its cousin lacking L2 interaction sites, the L1 $\gamma 2$ in $\gamma 8$ L2_GS
278 variant; see Figure 5C).

279

280 Overall, these results indicate that the long loop of $\gamma 8$ L1 is still able to modulate complexes at
281 extracellular sites with the receptor linker sites disrupted, supporting the idea that the linkers do not
282 function primarily to transduce distant TARP modulation. Rather, the LBD-TMD linkers are the
283 primary modulatory site for both $\gamma 8$ and $\gamma 2$. The latter has a short L1 loop, and cannot modulate
284 receptors if the L2 interaction is absent. However, $\gamma 8$ combines the longer L1 and the L2 site to
285 modulate receptor properties more effectively, in a compound fashion.

286

287 **Discussion**

288 The results we present here offer several new insights into TARP function. First of all, extracellular
289 sites account for all the modification of AMPA receptor gating by TARPs. Previous work showed
290 that L1 could transfer aspects of modulation between TARPs, but our experiments indicate that the
291 2nd short extracellular segment (L2), which varies strongly in sequence between TARPs, is
292 dominant. Further work will be required to establish the generality of this modulatory mechanism.

293

294 Secondly, these same sites do not have any appreciable role in determining assembly of TARP-
295 AMPA receptor complexes. Intuitively, this division of roles makes sense because gating
296 modification requires transient interactions on a timescale far faster than receptor assembly.

297 Therefore, interactions between transmembrane segments and intracellular regions are
298 responsible for assembly and modulation of polyamine block.

299

300 Thirdly, we show that the linkers to the transmembrane domain are key sites for modulation of
301 AMPA receptor gating by auxiliary proteins, and provide insights into the molecular basis of this
302 interaction. Previous work suggested ATD interactions and prominent roles for the LBD in
303 modulation, but the interactions we demonstrate here are much more proximal to the channel gate
304 (25). We could show a very close functional confluence between modifying the receptor itself and
305 modifying each TARP, at an interaction site predicted from structural modeling. The elimination of
306 modulation by nullifying L2 of γ_2 , or by mutating residues in the LBD-TMD linkers of GluA2,
307 strongly implicates this site as a pivotal interaction underlying modulation. Putative electrostatic
308 interactions posited from structural studies require a large conformational change (between 13 Å
309 and 25 Å depending on the TARP's position in the complex; measured between C-alpha atoms
310 from GluA2 K699 and γ_2 D92 in cryo-EM complexes 5kbu and 5kk2, respectively) (34, 35). A key
311 point here is that these interactions are secondary to those involving L2 at the AMPAR linkers.
312 These interactions should occur readily for each auxiliary protein subunit, allowing a maximal 4:4
313 stoichiometry with minimal conformational change for γ_2 (Figure 8A) (35). For other auxiliary
314 proteins, for example γ_8 , the stoichiometry of the L2-linker interaction would vary with the number
315 of associated TARPs, but will not be limited by position of the TARP within the complex (Figure
316 8B). Finally, neutralization of the major part of the acidic patch strongly enhanced modulation of
317 gating by γ_2 , ruling out that negative charges here have a dominant role in modulation.

318

319 Fourth, we show that the long extracellular loop 1 of γ_8 is a very strong positive modulator of
320 AMPA receptor gating, whose influence is likely held in check by the substoichiometric combination
321 of γ_8 with the AMPA receptor (28). The subunit γ_8 slows receptor desensitization via L1. This loop
322 can produce a profound block of desensitization when transplanted to γ_2 , and probably interacts
323 state-specifically with the LBD dimer because of its substantial reach (for examples see Figures 1
324 and 8). Previous kinetic measurements suggest that superactivation is adopted by a minor

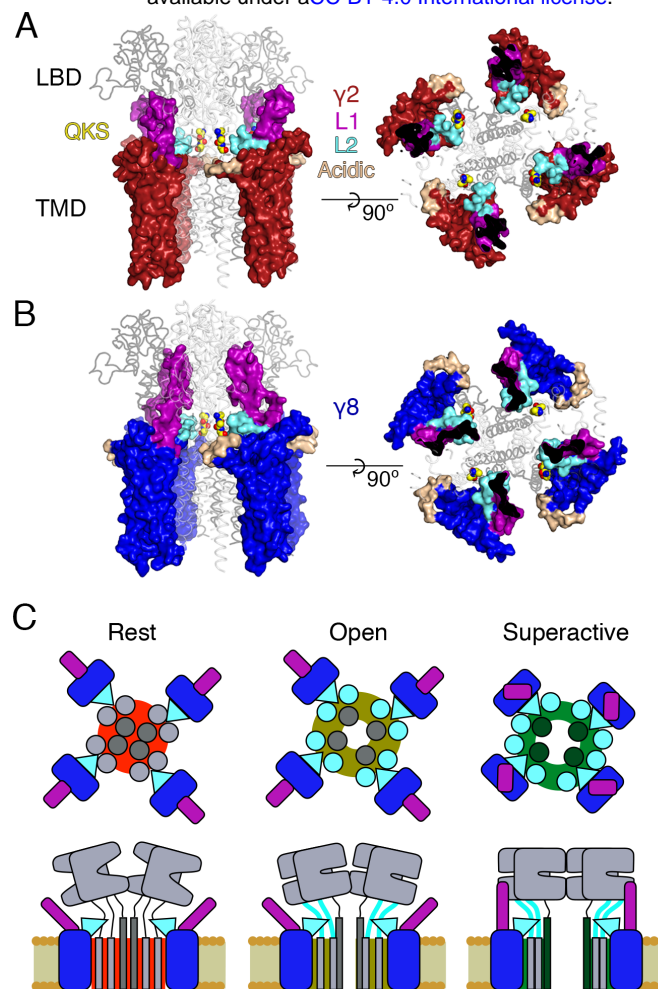


Figure 8. Proposed mechanism of AMPA modulation by TARPs. **A** Model of an AMPA- $\gamma 2$ complex in front view (*left*) and top view (*right*). Four molecules of $\gamma 2$ (*red*) are shown with L1 and L2 colored in magenta and cyan, respectively. L2 is sandwiched between the LBD-TMD connecting linkers of the receptor (grey, amino terminal domains omitted for clarity). The QKS sequence on the S1-M1 linker is shown as yellow atomic spheres. The acidic patch on the $\beta 4$ -TM2 linker is indicated in wheat. **B**) The model of $\gamma 8$ (*blue*) shows the similar interactions of L2 (*cyan*). The orientation of the more extensive loop 1 of $\gamma 8$ is not known, here it is depicted reaching up to the LBD dimer. **C**) Cartoon model of the proposed AMPA modulation mechanism, taking the example of $\gamma 8$. The AMPA-TARP complex is shown from top (upper panel) and in side view (lower panel). The receptor is colored in grey (pore forming M3 domain depicted in dark grey). $\gamma 8$ is colored as in panel B, with the acidic patch omitted. In the resting state (indicated by a red, closed pore) L2 is positioned in close proximity to the LBD-TMD connecting linkers. Once glutamate binds to the LBD, the resulting conformational change is transduced via the LBD-TMD linkers to open the pore (olive green, open state). During this transition L2 could wedge between the S1-M1 and S2-M4 linkers to modulate the receptor gating. The concerted action of L1 and L2 is necessary for superactivation of the receptor (dark green, high open probability state), most likely via L1 to stabilizing the LBDs layer.

326 population of receptors in equilibrium with saturating glutamate, speaking in favor of a weak
327 interaction that is boosted by the high effective concentration of L1 close to its site of action in the
328 receptor complex.

329

330 Our approach to fit Claudins with modeled loops from TARPs into the best resolution cryoEM
331 reconstruction available (5KK2, (35)) has clear implications for modulation. Our model, when
332 compared to the independently derived model of TARP-AMPA modulation (34), presents the
333 TARPs oriented at a subtly different angle. Therefore, our model predicted the L2 interaction on the
334 basis of one set of CryoEM data. We could not adequately incorporate the loops and the original
335 structures of the receptor linkers in this model (Figures 1 and S1). Whilst this problem could be due
336 to deficits in our model, another explanation is that the linkers (S1-M1 and S2-M4) are disrupted
337 from their basal positions, and that the L2 loop can wedge between them. Upon activation, it is
338 expected that the linkers will move away from the overall pore axis, which could permit further
339 state-dependent interactions (See cartoon in Figure 8C).

340

341 Future structural studies may permit a more detailed view into the interactions between L2 and the
342 linker domains of AMPAR. Although Claudin structures allowed positioning of auxiliary proteins
343 with high confidence within CryoEM reconstructions, the loops that we have investigated here are
344 not resolved within these structures, possibly because they interact transiently and are otherwise
345 disordered. Although our peptide array suggested that stretches of L1 interact with the LBD, we
346 were not able to obtain co-crystal structures of peptides with monomeric or dimeric forms of the
347 GluA2 LBD. Nonetheless, knowledge of Claudin structures enabled us to make structurally
348 sympathetic substitutions into TARPs for functional experiments that did not disrupt expression or
349 assembly of complexes. These approaches are in contrast with most previous work which simply
350 swapped extracellular portions, including mismatching the folded portions of the TARP extracellular
351 domain. Two observations highlight the importance of sympathetic exchanges. First, some naive
352 deletions would be expected to alter TARP structure. The simple deletion of L2 would severely
353 disrupt the extracellular domain of $\gamma 2$ or $\gamma 8$, because this segment connects structured regions

354 separated by about 10 Å. Second, some deletion chimeras we made retained modulation, with the
355 most striking example being $\gamma 8 \Delta L1 L2_GS$, which retained a substantial steady state current
356 (Figure 6). The residual modulation could be related to the presence of a few residues from L1 in
357 the $\gamma 8 \Delta L1 L2_GS$ (see Figure 1 – Figure supplement 3). Without maintaining these residues, the
358 chimera did not express. This observation illustrates the sensitivity of domain boundaries in
359 TARPs.

360

361 Because our observations suggest that the AMPA receptor linkers are key to TARP modulation, it
362 is likely that chimeric receptors with altered linkers that exhibit constitutive gating are bad reporters
363 of the TARP-GluA modulation, although they clearly delineate assembly motifs (29). The molecular
364 nature of the interactions we have identified here raise the intriguing possibility that acute
365 disassembly of complexes, rather than modulation, might be the target of recent subtype specific
366 drugs (19, 20).

367

368 Our results allow us to construct a tentative model for the distinct forms of modulation that TARPs
369 produce (Figure 8C). The slow increase in glutamate efficacy, which we term superactivation, is
370 specified by the combination of L1 and L2, whereas the basal increase in steady state current
371 arises from L2 alone. We previously modeled the modulatory interaction between TARPs and the
372 AMPA receptor with single conformational change, but did not consider desensitization. The
373 concerted involvement of multiple loops suggests multiple conformational states are required to
374 describe the interaction, most notably in the case of $\gamma 8$. The greater conformational space that can
375 be explored by loop 1, and its strong connection to superactivation, indicate that these
376 conformational changes could relate to the slow transitions represented in the model of
377 superactivation (37). In contrast, conformational changes of the linker region of the AMPA receptor
378 upon opening will naturally lead to a state-dependent interaction with L2 of $\gamma 2$ or $\gamma 8$, because of
379 the direct proximity. A further level of complexity is that an intact L2 segment is required for the
380 strong superactivation induced by $\gamma 8$, but is not required at all for slow desensitization behavior
381 that the long L1 loop of $\gamma 8$ can produce. Because in these experiments, slow desensitization

382 occurs when occupancy of superactive states is low, we can quite reasonably assume that L1
383 adopts multiple conformations to stabilize separate functional states of the receptor, and that some
384 functional signatures require a concerted action of both loops. Additional stabilization of
385 desensitized states by the variable loop 1 is also likely (30).

386

387 This work has produced mutant TARPs and AMPA receptors that both lack modulatory properties,
388 and also those that have greatly enhanced modulation. Both these signatures of activity should be
389 useful tools for investigating TARP action in synapses, including understanding the relative
390 importance of assembly into complexes for anchoring (39) as opposed to kinetic modulation, for
391 clarifying the consequences of TARP modulation for short term plasticity (18), and for better
392 identifying TARPs in ternary complexes with other auxiliary subunits (17, 40).

393 **Materials and Methods**

394 **Molecular biology**

395 We used GluA2 flip receptors, unedited at the pore site (Q-containing) in the pRK vector also
396 expressing eGFP following an internal ribosomal entry site (IRES) sequence. Mouse γ 2 was the
397 kind gift of Susumu Tomita and was expressed from an IRES-dsRed construct as previously
398 described (37). Mouse γ 8 (the kind gift of Roger Nicoll) was expressed the same way. Point
399 mutations and chimeras were created by overlap PCR and confirmed by double-stranded
400 sequencing. The construct boundaries of the chimeras used are shown in Figure 1 – Figure
401 supplement 3. Residues in GluA2 were numbered based on the assumption that the signal peptide
402 is 21 residues.

403

404 **Patch clamp electrophysiology**

405 Wild type or mutant GluA2 and TARP constructs were co-transfected in HEK 293 cells with PEI.
406 The ratios of co-transfection were 1:2 for GluA2- γ 2 and 1:5 for GluA2- γ 8, up to 2 μ g total DNA per
407 35 mm dish. The same ratios were maintained for all the reciprocal mutants. Cells were
408 supplemented with 40 μ M NBQX to reduce TARP-induced cytotoxicity. Recordings were performed
409 24-48 hours after transfection. The external recording solution contained (in mM): 150 NaCl, 0.1
410 $MgCl_2$, 0.1 $CaCl_2$ and 5 HEPES, titrated to pH 7.3 with NaOH. The pipette solution contained (in
411 mM): 120 NaCl, 10 NaF, 0.5 $CaCl_2$, 5 Na_4BAPTA , 5 HEPES and 0.05 spermine, pH 7.3. 10 mM
412 glutamate was applied to outside-out patches with a piezo-driven fast perfusion system (PI,
413 Germany). In order to isolate currents exclusively mediated by TARPed receptors, patches were
414 voltage-clamped at a holding potential of +50 mV. Currents were low-pass filtered at 5 kHz using
415 an Axopatch 200B amplifier (Molecular Devices, U.S.A.) and acquired with Axograph X software
416 (Axograph Scientific, U.S.A.). Typical 10-90% solution exchange times were faster than 300 μ s, as
417 measured from junction potentials at the open tip of the patch pipette.

418 *Data analysis.* To measure receptor desensitization we applied 10 mM glutamate for 500
419 ms. Desensitization rate and steady-state current were then obtained by fitting the traces with a
420 sum of two, and when necessary three, exponentials. Rates constants are expressed as weighted

421 mean of multiple components. Superactivation was measured during a 7 second application of
422 glutamate and was defined as the excess steady-state amplitude following the desensitization
423 trough, normalized to the peak current. A triple exponential function was used to fit the slowly
424 augmenting current of superactivation measurements. To account for possible variability in the
425 response and expression of the complexes, we tried to record at least 5-6 patches from at least
426 three different transfections for each condition. For experiments with very low success rates (that
427 is, worse than 1 patch in 20 giving an acceptable recording), in the presence of $\gamma 8$, at least three
428 patches were collected. No data were excluded, except from patches where recordings were
429 unstable, had excessive rundown or solution exchange slower than 0.5 ms as measured after the
430 experiment. Results are shown as mean \pm standard error of the mean (s.e.m.) and statistical
431 significance was assessed with a two-tailed Student's *t*-test as specified in Table 1.

432

433 **Protein expression and purification of soluble LBDs**

434 Using the flop isoform of rat GluA2 ligand binding domain (S1S2 fusion) in pET22b vector (kindly
435 provided by E. Gouaux) as a base, we inserted the flip mutations N744T, A745P, N754S, L758V,
436 and added the C-terminal residues Lys776-Gly779 (GluA2_LBD) and the non-desensitizing
437 mutation L483Y (GluA2_LBD_LY) by overlap mutagenesis. Protein expression and purification was
438 carried out as described previously (41). Briefly, monomeric and dimeric (L483Y) LBDs were
439 expressed in *E. coli* Origami B (DE3). Cells were harvested by centrifugation, lysed and subjected
440 to metal affinity chromatography and size exclusion chromatography. Fractions containing the N-
441 terminal His₈-tagged protein were pooled and dialysed against protein buffer (20 mM Tris pH7.4,
442 150 mM, NaCl, 10 mM glutamate). The purity was determined to >98% by SDS-PAGE analysis.

443

444 **Peptide spot array**

445 Peptides covering the extracellular parts of $\gamma 2$ and $\gamma 8$ were spotted onto amino modified Whatman
446 cellulose membranes (Figure 1B and Figure 1 – Figure supplement 1C) using a fully automatic
447 Spot synthesizer (Intavis, Köln, Germany). The spot array consisted of hexameric overlapping

448 peptides shifted by one residue. Peptide spotted membranes were rinsed with ethanol for 5
449 minutes, following three times 10 min washing with TBS and incubation with blocking buffer
450 (Casein Blocking buffer (Sigma B6429), 150 mM Saccharose, in TBS) for 3 hours at RT. The
451 blocking buffer was removed by three wash steps with TBS before the membranes were incubated
452 overnight at 4°C with either 50 µg/ml protein (GluA2_LBD or GluA2_LBD_LY) in blocking buffer or
453 blocking buffer only for control. Membranes were washed three times in TBS and incubated for 1.5
454 hours at RT with anti-poly_His Antibody (Sigma H1029) diluted 1:6000 in blocking solution followed
455 by three washes (a' 10 min) with TBS. Finally, membranes were incubated for 1.5 hours at RT with
456 HRP-conjugated anti-mouse IgG Antibody (Sigma A5906; 1:1000 dilution in blocking buffer) and
457 washed with TBS (three times a' 10 min). Visualization of protein-binding was carried out using a
458 chemo-luminescence substrate (Pierce™ ECL, ThermoFisher Scientific) and a Lumi-Imager™
459 instrument (Boehringer Mannheim, Germany). Spot-signal intensities were measured in Boehringer
460 Light Units (BLU) and the software GeneSpotter 2.6.0 (MicroDiscovery, Berlin, Germany) was
461 applied for data processing. Hits from peptides located within β-sheets were taken to be false
462 positives, because when isolated these peptides likely form unphysiological β-sheets in a non-
463 specific manner with existing structures in the GluA2 LBD. To have an idea about reproducibility of
464 this assay, we performed it twice with comparable results (source data is provided). The negative
465 control showed no signal, indicating no unspecific binding of the anti-poly His to the peptides.

466

467 **Structural modeling**

468 Initial γ2 and γ8 models were generated based on the crystal structure of claudin15 (PDB code:
469 4p79) using the SWISS-MODEL (42) and ProtMod server (part of the FFAS server, (43). Both
470 models were incomplete (either lacking linker structures or failing to correctly trace transmembrane
471 helix 3, TM3). Thus, we used COOT (version 0.8.7) to superpose the two generated models and to
472 build the final model with an intact helix 3 and plausible extracellular loops 1 and 2. Superposing
473 our final TARP models onto the γ2 molecules present in the AMPA-TARP cryo-EM structure (PDB
474 code: 5kk2) in PyMOL (v1.6.0.0) yielded in the AMPA-TARP complexes shown in our Figures. The

475 different possible orientations of Loop 1 were modeled using COOT. Unfortunately the LBD to TMD
476 connecting linkers (S1-TM1 and S2-TM4) are not resolved in the AMPA-TARP cryo-EM structure.
477 To better understand the Loop 2 participation in AMPA receptor regulation we used the crystal
478 structure of GluA2 (PDB code: 3kg2) with resolved linkers and superposed it onto the receptor of
479 our AMPA-TARP complex model (Figure 1 – Figure supplement 2). As the side chains of the
480 possible interacting residues (507-QKS-510, 781KSK-783) located in the LBD-TMD linkers were
481 not resolved in 3kg2 we modeled the most likely side chain conformations of these residues
482 (Figures 7A and B). All figures were prepared with PyMOL or IGOR Pro.

483

484

485 **Acknowledgements**

486 This work was funded by the Deutsche Forschungsgemeinschaft (DFG) – FOR 2518 (“Dynlon”, to
487 A.J.R.P.), the DFG Cluster of Excellence “NeuroCure” (DFG EXC-257, to ALC), and an Erwin-
488 Schrödinger Postdoctoral Fellowship (J3682-B21) of the Austrian Science fund (FWF, to C.E). We
489 thank Marcus Wietstruk and Ronny Schäfer for technical assistance.

490

491 **Competing Interests**

492 The authors declare no financial or non-financial competing interests.

493

494

495 **List of supplementary figures**

- 496 • Figure 1 - Figure supplement 1. Loop interactions between TARPs and GluA2.
- 497 • Figure 1 - Figure supplement 2. The acidic patch on β 4-TM2 of γ 2 negatively modulates
- 498 AMPA receptor gating.
- 499 • Figure 1 - Figure supplement 3. Sequence alignment of γ 2 and γ 8 constructs.
- 500 • Figure 2 - Figure supplement 1. Relief of polyamine block is not affected by loop mutations
- 501 in γ 2 and γ 8.
- 502 • Figure 7 - Figure supplement 1. GluA2 linker mutants do not affect receptor kinetics or
- 503 assembly with TARPs.

504

505 **List of source data files**

- 506 • Figure 1 – Source Data 1 : spot array quantitation
- 507 • Figure 1-Figure Supplement 2-Source Data 1 : rectification indices for negative patch
- 508 chimera
- 509 • Table 1 – Source Data 1 : kinetics and steady state currents from electrophysiological
- 510 recordings
- 511 • Figure 2 –Figure Supplement 1-Source Data 1 : rectification indices for electrophysiological
- 512 recordings of TARP chimeras
- 513 • Figure 6-Source Data 1 : rectification indices for electrophysiological recordings of TARP
- 514 deletion chimeras.
- 515 • Figure 7-Figure Supplement 1-Source Data 1 : rectification indices for electrophysiological
- 516 recordings of TARPs with GluA2 mutants.

517

518 **References**

- 519 1. Chen L, Chetkovich DM, Petralia RS et al. Stargazin regulates synaptic targeting of AMPA
520 receptors by two distinct mechanisms. *Nature*. 2000;408:936-943.
- 521 2. Schwenk J, Harmel N, Brechet A et al. High-resolution proteomics unravel architecture and
522 molecular diversity of native AMPA receptor complexes. *Neuron*. 2012;74:621-633.
- 523 3. Tomita S, Chen L, Kawasaki Y et al. Functional studies and distribution define a family of
524 transmembrane AMPA receptor regulatory proteins. *J Cell Biol*. 2003;161:805-816.
- 525 4. Dakoji S, Tomita S, Karimzadegan S, Nicoll RA, Brecht DS. Interaction of transmembrane
526 AMPA receptor regulatory proteins with multiple membrane associated guanylate kinases.
527 *Neuropharmacology*. 2003;45:849-856.
- 528 5. Yamazaki M, Fukaya M, Hashimoto K et al. TARPs gamma-2 and gamma-7 are essential for
529 AMPA receptor expression in the cerebellum. *Eur J Neurosci*. 2010;31:2204-2220.
- 530 6. Priel A, Kollerker A, Ayalon G, Gillor M, Osten P, Stern-Bach Y. Stargazin reduces
531 desensitization and slows deactivation of the AMPA-type glutamate receptors. *J Neurosci*.
532 2005;25:2682-2686.
- 533 7. von Engelhardt J, Mack V, Sprengel R et al. CKAMP44: a brain-specific protein attenuating
534 short-term synaptic plasticity in the dentate gyrus. *Science*. 2010;327:1518-1522.
- 535 8. McGee TP, Bats C, Farrant M, Cull-Candy SG. Auxiliary Subunit GSG1L Acts to Suppress
536 Calcium-Permeable AMPA Receptor Function. *J Neurosci*. 2015;35:16171-16179.
- 537 9. Rouach N, Byrd K, Petralia RS et al. TARP gamma-8 controls hippocampal AMPA receptor
538 number, distribution and synaptic plasticity. *Nat Neurosci*. 2005;8:1525-1533.
- 539 10. Soto D, Coombs ID, Kelly L, Farrant M, Cull-Candy SG. Stargazin attenuates intracellular
540 polyamine block of calcium-permeable AMPA receptors. *Nat Neurosci*. 2007;10:1260-1267.
- 541 11. Kato AS, Zhou W, Milstein AD et al. New transmembrane AMPA receptor regulatory protein
542 isoform, gamma-7, differentially regulates AMPA receptors. *J Neurosci*. 2007;27:4969-4977.
- 543 12. Bats C, Soto D, Studniarczyk D, Farrant M, Cull-Candy SG. Channel properties reveal
544 differential expression of TARPed and TARPless AMPARs in stargazer neurons. *Nat*
545 *Neurosci*. 2012;15:853-861.
- 546 13. Tomita S, Fukata M, Nicoll RA, Brecht DS. Dynamic interaction of stargazin-like TARPs with
547 cycling AMPA receptors at synapses. *Science (New York, NY)*. 2004;303:1508-1511.
- 548 14. Boudkkazi S, Brechet A, Schwenk J, Fakler B. Cornichon2 dictates the time course of
549 excitatory transmission at individual hippocampal synapses. *Neuron*. 2014;82:848-858.
- 550 15. Milstein AD, Zhou W, Karimzadegan S, Brecht DS, Nicoll RA. TARP subtypes differentially and
551 dose-dependently control synaptic AMPA receptor gating. *Neuron*. 2007;55:905-918.
- 552 16. Klaassen RV, Stroeder J, Coussen F et al. Shisa6 traps AMPA receptors at postsynaptic
553 sites and prevents their desensitization during synaptic activity. *Nat Commun*. 2016;7:10682.

- 554 17. Khodosevich K, Jacobi E, Farrow P et al. Coexpressed auxiliary subunits exhibit distinct
555 modulatory profiles on AMPA receptor function. *Neuron*. 2014;83:601-615.
- 556 18. Devi SPS, Howe JR, Auger C. Train stimulation of parallel fibre to Purkinje cell inputs reveals
557 two populations of synaptic responses with different receptor signatures. *J Physiol*.
558 2016;594:3705-3727.
- 559 19. Maher MP, Wu N, Ravula S et al. Discovery and Characterization of AMPA Receptor
560 Modulators Selective for TARP- γ 8. *J Pharmacol Exp Ther*. 2016;357:394-414.
- 561 20. Kato AS, Burris KD, Gardinier KM et al. Forebrain-selective AMPA-receptor antagonism
562 guided by TARP γ -8 as an antiepileptic mechanism. *Nat Med*. 2016;22:1496-1501.
- 563 21. Tomita S, Adesnik H, Sekiguchi M et al. Stargazin modulates AMPA receptor gating and
564 trafficking by distinct domains. *Nature*. 2005;435:1052-1058.
- 565 22. Tomita S, Shenoy A, Fukata Y, Nicoll RA, Brecht DS. Stargazin interacts functionally with the
566 AMPA receptor glutamate-binding module. *Neuropharmacology*. 2007;52:87-91.
- 567 23. Cho C-H, St-Gelais F, Zhang W, Tomita S, Howe JR. Two families of TARP isoforms that
568 have distinct effects on the kinetic properties of AMPA receptors and synaptic currents.
569 *Neuron*. 2007;55:890-904.
- 570 24. Soto D, Coombs ID, Renzi M, Zonouzi M, Farrant M, Cull-Candy SG. Selective regulation of
571 long-form calcium-permeable AMPA receptors by an atypical TARP, gamma-5. *Nat Neurosci*.
572 2009;12:277-285.
- 573 25. Cais O, Herguedas B, Krol K, Cull-Candy SG, Farrant M, Greger IH. Mapping the Interaction
574 Sites between AMPA Receptors and TARPs Reveals a Role for the Receptor N-Terminal
575 Domain in Channel Gating. *Cell Rep*. 2014;9:728-740.
- 576 26. Shi Y, Lu W, Milstein AD, Nicoll RA. The stoichiometry of AMPA receptors and TARPs varies
577 by neuronal cell type. *Neuron*. 2009;62:633-640.
- 578 27. Kim KS, Yan D, Tomita S. Assembly and stoichiometry of the AMPA receptor and
579 transmembrane AMPA receptor regulatory protein complex. *J Neurosci*. 2010;30:1064-1072.
- 580 28. Hastie P, Ulbrich MH, Wang H-L et al. AMPA receptor/TARP stoichiometry visualized by
581 single-molecule subunit counting. *Proc Natl Acad Sci U S A*. 2013
- 582 29. Ben-Yaacov A, Gillor M, Haham T, Parsai A, Qneibi M, Stern-Bach Y. Molecular Mechanism
583 of AMPA Receptor Modulation by TARP/Stargazin. *Neuron*. 2017;93:1126-1137.e4.
- 584 30. Twomey EC, Yelshanskaya MV, Grassucci RA, Frank J, Sobolevsky AI. Structural Bases of
585 Desensitization in AMPA Receptor-Auxiliary Subunit Complexes. *Neuron*. 2017;94:569-
586 580.e5.
- 587 31. Suzuki H, Nishizawa T, Tani K et al. Crystal Structure of a Claudin Provides Insight into the
588 Architecture of Tight Junctions. *304fullpdf*. 2014;344:304-307.
- 589 32. Wu J, Yan Z, Li Z et al. Structure of the voltage-gated calcium channel Cav1.1 complex.
590 *Science*. 2015;350:aad2395.

- 591 33. Shinoda T, Shinya N, Ito K et al. Structural basis for disruption of claudin assembly in tight
592 junctions by an enterotoxin. *Sci Rep.* 2016;6:33632.
- 593 34. Twomey EC, Yelshanskaya MV, Grassucci RA, Frank J, Sobolevsky AI. Elucidation of AMPA
594 receptor-stargazin complexes by cryo-electron microscopy. *Science.* 2016;353:83-86.
- 595 35. Zhao Y, Chen S, Yoshioka C, Bacongus I, Gouaux E. Architecture of fully occupied GluA2
596 AMPA receptor-TARP complex elucidated by cryo-EM. *Nature.* 2016
- 597 36. Kato AS, Gill MB, Ho MT et al. Hippocampal AMPA Receptor Gating Controlled by Both
598 TARP and Cornichon Proteins. *Neuron.* 2010;68:1082-1096.
- 599 37. Carbone AL, Plested AJR. Superactivation of AMPA receptors by auxiliary proteins. *Nat*
600 *Commun.* 2016;7:10178.
- 601 38. Dawe GB, Musgaard M, Arousseau MRP et al. Distinct Structural Pathways Coordinate the
602 Activation of AMPA Receptor-Auxiliary Subunit Complexes. *Neuron.* 2016;89:1264-1276.
- 603 39. Opazo P, Labrecque S, Tigaret CM et al. CaMKII triggers the diffusional trapping of surface
604 AMPARs through phosphorylation of stargazin. *Neuron.* 2010;67:239-252.
- 605 40. Herring B, Shi Y, Suh Y et al. Cornichon Proteins Determine the Subunit Composition of
606 Synaptic AMPA Receptors. *Neuron.* 2013;77:1083-1096.
- 607 41. Salazar H, Eibl C, Chebli M, Plested A. Mechanism of partial agonism in AMPA-type
608 glutamate receptors. *Nat Commun.* 2017;8:14327.
- 609 42. Arnold K, Bordoli L, Kopp J, Schwede T. The SWISS-MODEL workspace: a web-based
610 environment for protein structure homology modelling. *Bioinformatics.* 2006;22:195-201.
- 611 43. Jaroszewski L, Li Z, Cai XH, Weber C, Godzik A. FFAS server: novel features and
612 applications. *Nucleic Acids Res.* 2011;39:W38-44.

613

614

Construct	k_{des} (s ⁻¹)	p	I_{ss} (%)	p	Superact (%)	p
A2 wt	120 ± 15 (9)		5 ± 1		–	–
γ2	60 ± 5 (24)		25 ± 2		7 ± 2 (10)	
γ8	40 ± 5 (9)		25 ± 5		30 ± 6 (4)	
γ2 β4 TM2 §	40 ± 5 (7)	0.004	50 ± 5	1 × 10 ⁻⁵	17 ± 4 (5)	0.009
L1 γ8 in γ2 §	35 ± 5 (30)	5 × 10 ⁻⁶	50 ± 5	7 × 10 ⁻⁶	27 ± 6 (10)	0.003
L1 γ2 in γ8 §	45 ± 1 (28)	0.34	25 ± 3	0.86	16 ± 1 (16)	0.001
γ2 ΔL1 §	60 ± 5 (11)	0.90	15 ± 2	0.008	6 ± 2 (6)	0.52
γ8 ΔL1 §	60 ± 5 (15)	0.002	15 ± 3	0.03	16 ± 3 (6)	0.02
γ2 L2_GS §	65 ± 5 (15)	0.49	5 ± 1	1 × 10 ⁻⁶	1.3 ± 0.6 (8)	0.003
γ8 L2_GS §	25 ± 5 (6)	0.002	40 ± 4	0.07	12 ± 2 (4)	0.01
L1 γ8 in γ2 L2_GS §	10 ± 0.5 (7)	6 × 10 ⁻¹⁰	45 ± 3	6 × 10 ⁻⁵	4 ± 2 (6)	0.19
L1 γ2 in γ8 L2_GS §	85 ± 5 (6)	1 × 10 ⁻⁵	5 ± 1	0.001	1 ± 0.7 (6)	9 × 10 ⁻⁵
γ2 ΔL1 L2_GS §	80 ± 20 (5)	0.03	2 ± 1	4 × 10 ⁻⁴	0 (4)	0.011
γ8 ΔL1 L2_GS §	60 ± 10 (5)	0.02	10 ± 5	0.02	3 ± 1 (4)	0.02
A2 K509A Δ	100 ± 5 (5)	0.34	3 ± 0.5	0.71	–	–
A2 508GAG510 Δ	145 ± 35 (3)	0.42	1 ± 0.5	0.27	–	–
A2 781GSG783 Δ	110 ± 15 (3)	0.76	2 ± 1	0.46	–	–
A2 GAG/GSG Δ	150 ± 20 (5)	0.20	2 ± 1	0.44	–	–
A2 K509A + γ2 #	30 ± 10 (5)	3 × 10 ⁻⁴	45 ± 3	2 × 10 ⁻⁴	5 ± 5 (4)	0.59
A2 508GAG510 + γ2 #	70 ± 5 (4)	0.39	10 ± 5	0.07	0 (3)	0.03
A2 781GSG783 + γ2 #	60 ± 5 (9)	0.60	10 ± 1	0.001	2 ± 0.5 (8)	0.005
A2 GAG/GSG + γ2 #	80 ± 5 (8)	0.01	5 ± 1	9 × 10 ⁻⁵	0 (4)	0.01
A2 GAG/GSG + L1 γ8 in γ2 #	12 ± 0.5 (5)	4 × 10 ⁻⁸	30 ± 5	0.21	2 ± 2 (4)	0.065
A2 GAG/GSG + γ8 #	45 ± 2 (5)	0.30	12 ± 3	0.03	25 ± 5 (5)	0.37
A2 GAG/GSG + L1 γ2 in γ8 #	72 ± 5 (5)	8 × 10 ⁻⁵	4 ± 1	0.001	1 ± 1 (4)	0.001

615

616

617 **Table 1. Kinetic properties of wild type and chimeric TARPs and GluA2 linker mutants.** k_{des}

618 is rate of desensitization, I_{ss} the steady state current expressed as percentage of the peak current

619 and Superact the extent of superactivation expressed as the slow increase in steady state current

620 during prolonged exposure to glutamate (see Materials and Methods for details). The number of

621 patches recorded for each condition is shown in brackets. Values are shown as mean ± s.e.m. p

622 values (from Student's t test) are calculated as follows: § against the parent TARP; Δ against

623 GluA2 WT; # against GluA2 WT + TARP. Currents recorded in the presence of TARPs were held

624 at +50 mV in the presence of 50 μM spermine in the pipette solution. Recordings in the absence of

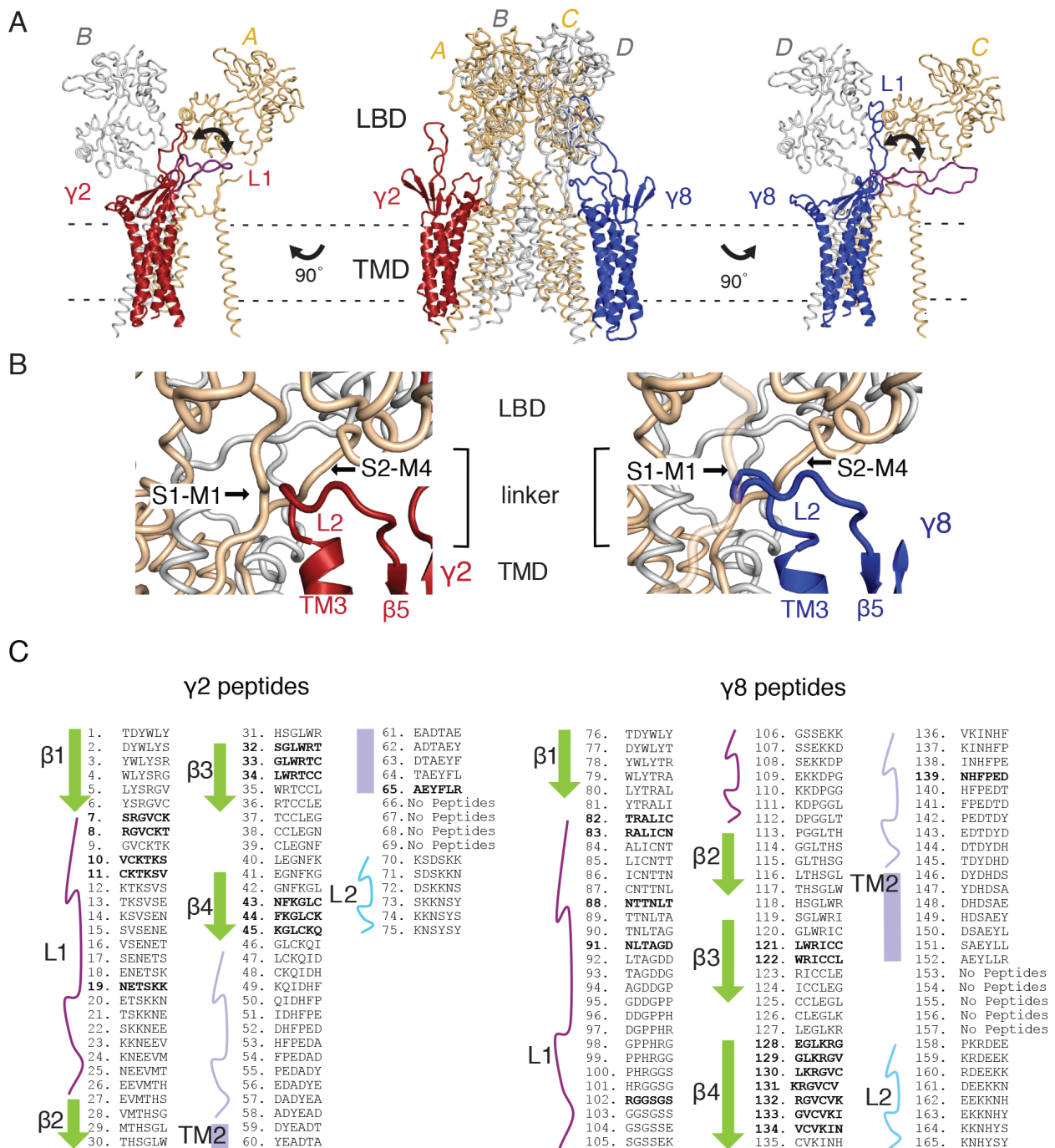
625 TARPs were done at –60 mV without intracellular polyamines. Source data for Table 1 is found in

626 Table 1 – Source Data 1

627

628

629 **Supplementary Figures**

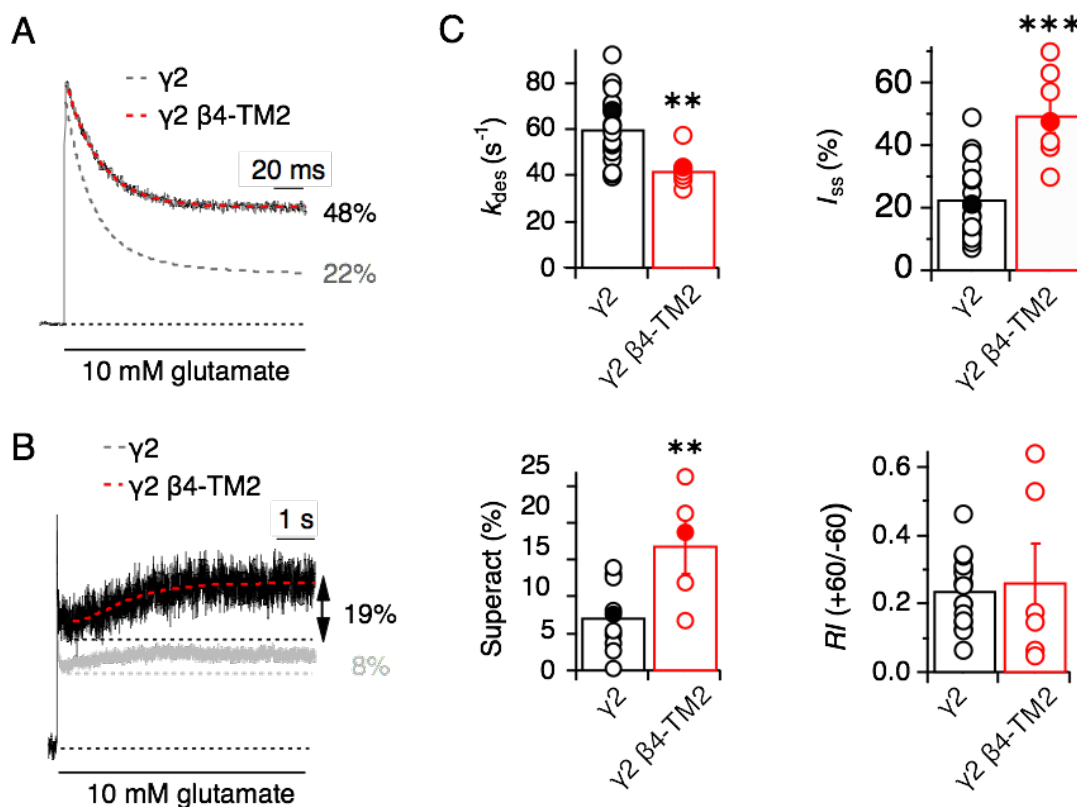


630

631 **Figure 1- Figure supplement 1. Loop interactions between TARPs and GluA2.**

632 **A)** The middle panel shows TARPs $\gamma 2$ (red) and $\gamma 8$ (blue) positioned between equivalent receptor
 633 subunits (A & B and C & D). We modeled L1 in two positions, either between the LBD dimer
 634 (colored as the respective TARP) or underneath the lower lobe of the LBD (purple; left panel $\gamma 2$,
 635 right panel $\gamma 8$). **B)** The model suggests L2 of both $\gamma 2$ (red, left panel) and $\gamma 8$ (blue, right panel)
 636 engages in similar interactions, independent from the TARP's location in the complex. L2 is

637 sandwiched between the receptor linkers (S1-M1 and S2-M4) connecting the LBD to the pore-
638 forming TMD. **C)** Sequences of the hexameric TARP peptides used in the peptide mapping array
639 are listed according to their position in the array. Secondary structure elements are shown in the
640 same color code as in Figures 1B and C. Peptide sequences and quantitation are found in Figure
641 1–Source Data 1. Positive peptide hits are indicated as bold sequences.



642

643 **Figure 1- Figure supplement 2. The acidic patch on $\beta 4$ -TM2 of $\gamma 2$ negatively modulates**
 644 **AMPA receptor gating.**

645 **A)** Representative traces from $\gamma 2$ $\beta 4$ -TM2 coexpressed with GluA2 (red; 3 negative charges
 646 removed) in response to a 500 ms pulse of 10 mM Glutamate show a substantial reduction in
 647 desensitization rate and extent ($k_{des} = 43 \text{ s}^{-1}$; $I_{ss} = 48 \%$) compared to wild-type $\gamma 2$ (dashed grey
 648 line). The mutations in $\gamma 2$ $\beta 4$ -TM2 were D88G, E90S and D92G. **B)** Neutralizing the negative patch
 649 on the $\beta 4$ -TM2 increased $\gamma 2$ -mediated superactivation more than two-fold. The grey trace
 650 represents wild type $\gamma 2$. **C)** Bar graphs showing the effects of neutralization of the $\gamma 2$ negative
 651 patch on desensitization, steady-state current, superactivation. The rectification index was not
 652 changed, indicating relief of polyamine block was intact. Filled symbols correspond to the traces
 653 shown in A) and B). $**p < 0.01$, $***p < 0.001$, against $\gamma 2$. Source data for kinetic data in panel C is
 654 found in Table 1 – Source Data 1. Source data for rectification indices in panel C is found in Figure
 655 1 – Figure Supplement 2 – Source Data 1. Error bars represent s.e.m.

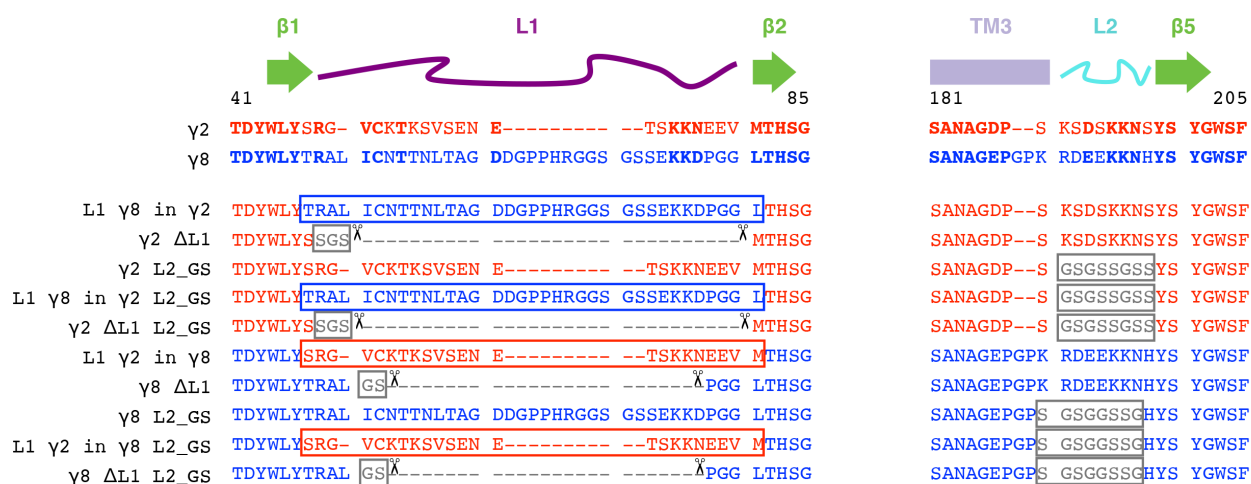
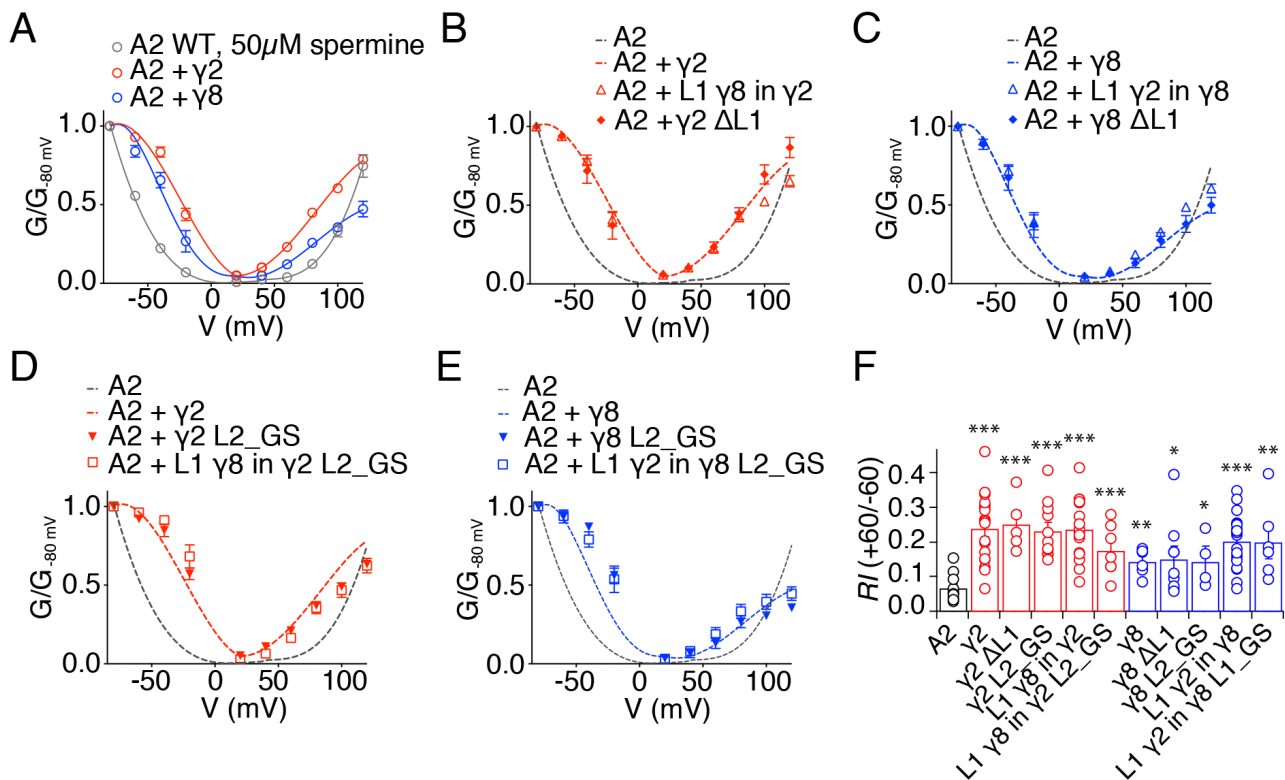


Figure 1- Figure supplement 3. Sequence alignment of $\gamma 2$ and $\gamma 8$ constructs.

The sequences of the extracellular regions Loop1 (L1, purple) and Loop2 (L2, cyan) of $\gamma 2$ (red) and $\gamma 8$ (blue) are aligned with the secondary structural elements on top. Constructs carrying deletions (L1, indicated by scissors), neutralization (L2, glycine-serine (GS)-Linker) and chimeras (switching L1 between the TARPs) and combinations of these are shown below.

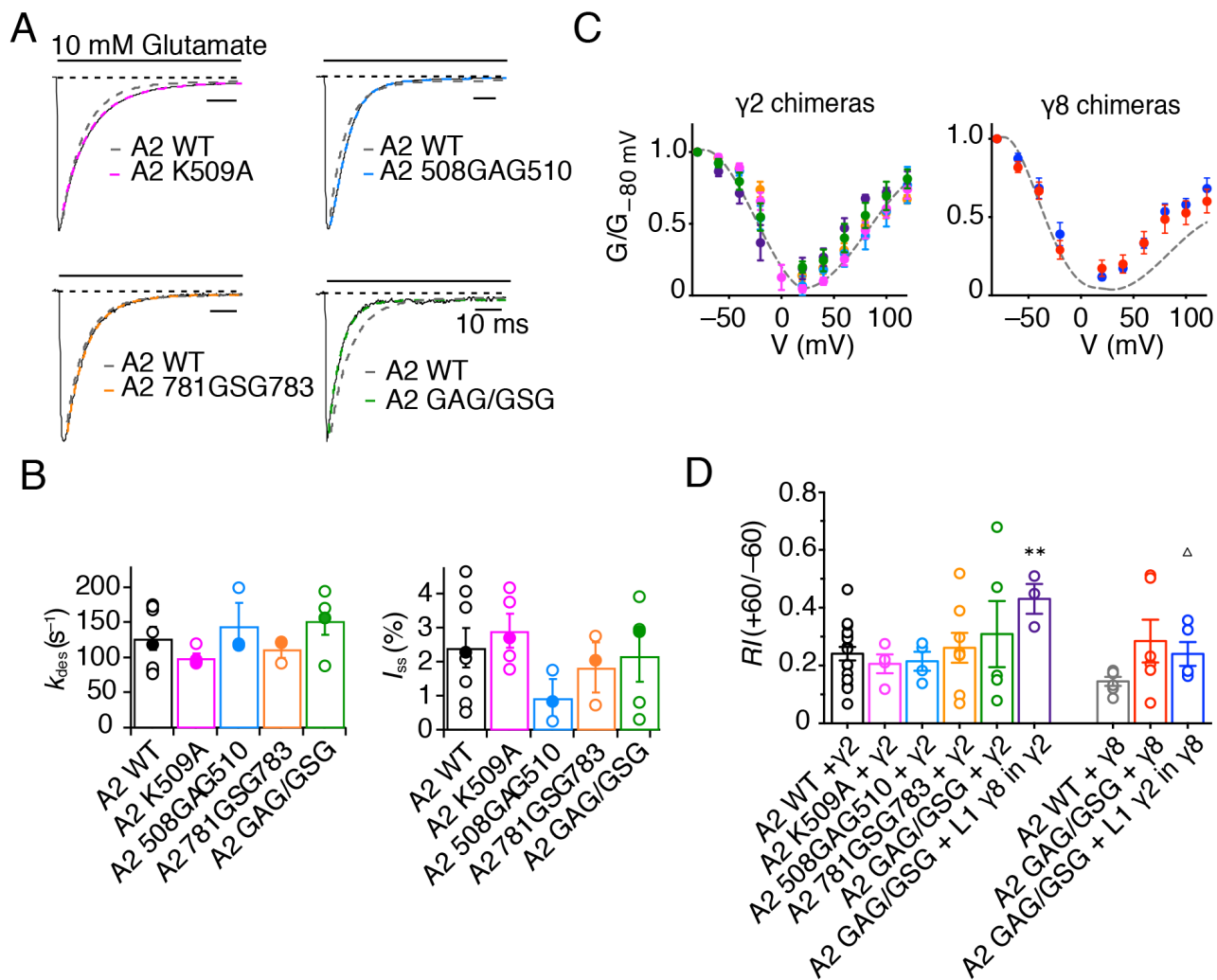


662

663 **Figure 2 Figure supplement 1. Relief of polyamine block is not affected by loop mutations**

664 **in γ 2 and γ 8.**

665 **A)** Normalised conductance-voltage plots show that TARP γ 2 (*red*) is better at relieving the
666 polyamine (PA) block of unedited GluA2 receptors (*grey*) than γ 8 (*blue*). **B)** Relief of PA block by
667 γ 2 L1 mutants (*filled symbols*) is indistinguishable from that of the wild type construct (*dashed line*).
668 GluA2 WT is shown in grey for comparison. **C)** Replacing L1 of γ 8 with that of γ 2 or deleting it does
669 not affect its ability to relieve PA block of GluA2(Q) receptors. **D)** Neutralizing L2 in γ 2, alone or in
670 combination with L1 from γ 8, does not affect PA block. **E)** Neutralizing L2 in γ 8 and in γ 8 with L1
671 from γ 2 show similar PA block relief as γ 8 wild type. **F)** Bar graph summarizing the rectification
672 index (RI, calculated as the ratio between the current recorded at +60 mV and that recorded at -60
673 mV) of γ 2 (in *red*) and γ 8 (in *blue*) loop mutants coexpressed with GluA2(Q). Currents were
674 recorded in the presence of 50 μ M spermine in the pipette solution. * $p < 0.05$, ** $p < 0.01$, *** $p <$
675 0.001, against GluA2(Q). Source data for panel F is found in Figure 2 – Figure supplement 1 –
676 Source Data 1. Error bars represent s.e.m.



677

678 **Figure 7-Figure supplement 1. GluA2 linker mutants do not affect receptor kinetics or**

679 **assembly with TARPs.**

680 **A)** Representative traces from GluA2 linker mutants in response to 500 ms pulses of 10 mM

681 Glutamate. GluA2 WT is shown in grey. **B)** Bar graph summarizing the desensitization kinetics and

682 the level of steady state current for GluA2 linker mutants. Filled dots represent the traces shown in

683 **A).** **C) and D)** GV responses and rectification index for GluA2 mutants in complex with $\gamma 2$ WT or L1

684 $\gamma 8$ in $\gamma 2$ chimera (*left*) and $\gamma 8$ WT and L1 $\gamma 2$ in $\gamma 8$ chimera (*right*). ** $p < 0.01$, against $\gamma 2$; $\Delta p <$

685 0.05, against $\gamma 8$. Source data for panel C is found in Table 1 – Source Data 1 and source data for

686 panel D is found in Figure 7 – Figure supplement 1 – Source Data 1. Error bars represent s.e.m.